



**HAL**  
open science

## **In-situ dissolution rates of silicate minerals and associated bacterial communities in the critical zone (Strengbach catchment, France)**

Bastien Wild, Damien Daval, Emilie Beaulieu, Marie-Claire Pierret, Daniel Viville, Gwenael Imfeld

► **To cite this version:**

Bastien Wild, Damien Daval, Emilie Beaulieu, Marie-Claire Pierret, Daniel Viville, et al.. In-situ dissolution rates of silicate minerals and associated bacterial communities in the critical zone (Strengbach catchment, France). *Geochimica et Cosmochimica Acta*, 2019, 249, pp.95-120. 10.1016/j.gca.2019.01.003 . hal-02988804

**HAL Id: hal-02988804**

**<https://hal.science/hal-02988804>**

Submitted on 12 Nov 2020

**HAL** is a multi-disciplinary open access archive for the deposit and dissemination of scientific research documents, whether they are published or not. The documents may come from teaching and research institutions in France or abroad, or from public or private research centers.

L'archive ouverte pluridisciplinaire **HAL**, est destinée au dépôt et à la diffusion de documents scientifiques de niveau recherche, publiés ou non, émanant des établissements d'enseignement et de recherche français ou étrangers, des laboratoires publics ou privés.



# *In-situ* dissolution rates of silicate minerals and associated bacterial communities in the critical zone (Strengbach catchment, France)

Bastien Wild<sup>a,b,\*</sup>, Damien Daval<sup>a</sup>, Emilie Beaulieu<sup>a</sup>, Marie-Claire Pierret<sup>a</sup>  
Daniel Viville<sup>a</sup>, Gwenaël Imfeld<sup>a</sup>

<sup>a</sup> Laboratoire d'Hydrologie et de Géochimie de Strasbourg (LHyGeS), Université de Strasbourg /EOST-ENGEEES-CNRS UMR 7517, 1 Rue Blessig, 67000 Strasbourg, France

<sup>b</sup> Andlinger Center for Energy and the Environment, Princeton University, 86 Olden Street, Princeton, NJ 08544, USA

Received 26 February 2018; accepted in revised form 1 January 2019; Available online 14 January 2019

## Abstract

The weathering of silicate minerals in the Critical Zone (CZ) is fundamental for numerous environmental and societal issues. Despite decades of efforts to accurately record biogeochemical variables controlling mineral reactivity in the field and to reproduce them in the laboratory, weathering rate estimates still differ from those observed in natural settings. Here we examine the biogeochemical environment of mineral surfaces exposed to contrasted weathering conditions in various compartments of a temperate CZ (Strengbach observatory, France). A novel approach was developed to probe both *in-situ* mineral dissolution rates and bacterial diversity associated with mineral surfaces. Labradorite and olivine minerals were either buried in the A and C horizons of a soil profile, directly exposed to meteoric fluids or immersed in stream water. Dissolution rates recorded in the soil profile were up to 2 orders of magnitude slower than those predicted using a numerical weathering model. Samples directly exposed to meteoric fluids exhibited contrasted dissolution rates that could not be explained by simple abiotic weathering, while dissolution rates of samples incubated in stream water were particularly low. In soil profiles, the field-laboratory discrepancy by up to 2 orders of magnitude was attributed to heterogeneity of fluid circulation and local variation of reaction conditions. Mineral substrates changed bacterial communities of the mineralosphere after 9 and 20 months of incubation in the CZ. However, we observed that this effect could be delayed or driven by extrinsic factors. Although mineral probes in soil horizons were enriched in bacterial phylotypes potentially involved in mineral weathering (e.g., *Pseudomonas* sp., *Collimonas* sp., *Burkholderia* sp., *Janthinobacterium* sp., *Leifsonia* sp., and *Arthrobacter* sp.), the relative contribution of biotic weathering could not be quantified *in-situ*. Altogether, the heterogeneity of *in-situ* mineral dissolution rates in compartments of the CZ underscores the need to improve spatial characterization of hydrogeochemical properties at the soil profile scale, and to evaluate quantitatively the role of microbial communities in mineral weathering.

© 2019 Elsevier Ltd. All rights reserved.

**Keywords:** Critical zone; Silicate weathering; Bacterial communities; Mineral dissolution; Microbial diversity; Forested catchment; Feldspar; Olivine; Quartz

## 1. INTRODUCTION

The weathering of primary minerals and associated fluxes involved in elemental cycling in natural settings are relevant for numerous environmental and societal

\* Corresponding author at: Andlinger Center for Energy and the Environment, Princeton University, 86 Olden Street, Princeton, NJ 08544, USA.

E-mail address: [bwild@princeton.edu](mailto:bwild@princeton.edu) (B. Wild).

challenges. Important issues include the management of inorganic nutrients stocks in soils with the development of sustainable agricultural and forestry practices (Klaminder et al., 2011; Lucas et al., 2011; van der Heijden et al., 2013; Johnson et al., 2015), the contamination of ecosystems due to mining activities (Yu et al., 2014), or long-term forecast of atmospheric CO<sub>2</sub> concentrations (Beaulieu et al., 2012).

Studies on (bio)weathering rates at global (Gaillardet et al., 1999), regional (Negrel et al., 1993; Gaillardet et al., 1995), local (Feger et al., 1990; Augusto et al., 2000; Klaminder et al., 2011) or micro scales (Fischer et al., 2012; Bonneville et al., 2016; Li et al., 2016) underscore that knowledge of mineral dissolution rates in the critical zone (CZ) remains incomplete. Field weathering rates are usually determined with indirect methods, such as measurements of U-series nuclides in soils and weathering profiles (Ackerer et al., 2016), the monitoring of changes in solid-state regolith compositions (White et al., 1996) and/or geochemical mass-balances over large space and time scales (Velbel, 1993). These rates are often inconsistent with those measured in the laboratory (White and Brantley, 2003). This “field-lab discrepancy” (Paces, 1983; White and Brantley, 2003; Zhu et al., 2014) has stimulated intensive research to reduce uncertainties on element budgets in natural settings. For instance, several types of indirect field measurement approaches were combined to yield estimates of *in-situ* mineral weathering rates (Ferrier et al., 2010; Ackerer et al., 2016). In parallel, mineral dissolution kinetics were evaluated in the laboratory by monitoring dissolution rates against controlled parameters, such as T, pH or  $\Delta G_r$  (Carroll and Knauss, 2005; Hellmann and Tisserand, 2006; Gruber et al., 2014). This framework allowed to build up databases of parameters used in semi-empirical mineral weathering rate laws (Palandri and Kharaka, 2004; Rimstidt et al., 2012). While this overall strategy has the merit to combine data from independent “top-down” (field measurements) and “bottom-up” (lab experiments) approaches, a consistent theory for mineral weathering in the field is still missing. One possible reason is that “top-down” and “bottom-up” approaches consider different processes, which are recorded on distinct temporal and spatial scales.

Most field studies integrate mineral weathering over large space scales, which do not capture the details of the biogeochemical processes at stake. Field studies may thus fail to provide a mechanistic understanding of *in-situ* mineral weathering, although relevant data for past and current weathering in the critical zone have been produced. Estimates of field weathering rates remain, however, several orders of magnitude greater than laboratory estimates used in common rate laws in reactive transport models (White and Brantley, 2003; Maher et al., 2004).

In addition, inconsistent timescales considered in the laboratory and in the field may result in contrasted mineral dissolution rates due to intrinsic factors, i.e. related to the intrinsic crystal chemistry of the weathered phase, or extrinsic factors, i.e. related to the reacting environment of the crystal (White and Brantley, 2003; Beig and Luttge, 2006; Gruber et al., 2014). Indeed, the physicochemical properties of the fluid/silicate interface may change over time during

mineral dissolution, depending on weathering conditions (Daval et al., 2011; Wild et al., 2016). As a result, the dissolution rate of mineral surfaces aged in the field over geologic time scales cannot be directly compared to that of pristine mineral surfaces used in the laboratory, resulting in inconsistent estimates of mineral weathering rates. Moreover, silicate mineral dissolution is too slow under typical field conditions to be measured directly with sufficient accuracy. As a result, most studies on silicate dissolution kinetics have been restricted to the investigation of abiotic, far-from-equilibrium conditions (extreme pH and/or temperature conditions) in laboratory setups. These experimental conditions might change the nature of elementary processes actually driving mineral dissolution compared to those prevailing in the field.

To sum up, (i) mineral dissolution rates measured in the field and in the lab over contrasted time and space scales may not account for the same processes, (ii) local physicochemical environments controlling mineral dissolution rates in the CZ are difficult to probe, and (iii) laboratory conditions, which are generally controlled, homogeneous, constant and abiotic (or do not involve (multiple) (micro) organisms), may only partly reflect field processes. In that sense, the strict addition of numerous processes observed independently in simple laboratory set-ups (e.g., abiotic, high temperature, short timescales, etc.) may fail to reproduce mineral weathering in natural settings. Nevertheless, parameters derived from laboratory experiments are directly used in reactive transport codes (Yeh and Tripathi, 1991; Steefel and Lasaga, 1994; Gerard et al., 1996) or in chemical weathering models at the catchment scale (Sverdrup and Warfvinge, 1995; Godderis et al., 2006). Current models may thus partly fail to account for extrinsic and intrinsic processes, thereby limiting agreement between simulation outputs and measurements of field weathering rates.

While several models integrate element recycling by vegetation and soil acidity controlled by heterotrophic and autotrophic respiration (Godderis et al., 2006; Roelandt et al., 2010; Beaulieu et al., 2012), the influence of microorganisms on *in-situ* mineral dissolution is currently missing. However, microorganisms have been recognized to interact with mineral substrates (Bennett et al., 1996; Uroz et al., 2009, 2015), and to impact mineral weathering directly or indirectly. For instance, microorganisms can control locally the thermodynamic activity of species in solution by biofilm production (Barker and Banfield, 1996). Microorganisms can also produce organic molecules (either organic acids, ligands or siderophores), which may result in organic-metal chelation (Drever and Stillings, 1997) or ligand-promoted dissolution (Welch and Ullman, 1993; Ganor et al., 2009). Microorganisms can impact mineral weathering by modifying redox (Newman and Kolter, 2000; Lower et al., 2001; Reguera et al., 2005; Roden et al., 2010) or acid-base conditions (Alisa Mast and Drever, 1987), or even by inducing mechanical stress (Bonneville et al., 2009; Li et al., 2016). The effect of individual microbial strains on mineral weathering has been extensively characterized in controlled systems (Kalinowski et al., 2000; Brantley et al., 2001). However, this approach relies on

the selection of culturable strains, which accounts for much less than 1% of the microorganisms occurring in many environments (Solden et al., 2016). Some model microorganisms may thus be selected based on cultivation restrictions (van Scholl et al., 2008) rather than for their actual effect or relevance for mineral weathering. To date, most available bioweathering studies have been considering axenic cultures, with the exception of some recent attempts to use field-relevant microbial communities (e.g. Wild et al., 2018). In addition, planktonic cells are generally considered, while biofilms are often neglected in weathering studies. Altogether, this questions the environmental relevance of experiments conducted with model cultures to infer weathering rates under field conditions. Identifying the weathering potential of microbial communities and their contribution to global weathering fluxes remains a challenging but fundamental issue.

Another important gap between laboratory and field conditions is the consideration of microbial communities in nutrient-poor environments. While microorganisms influence mineral dissolution rates, the mineral substratum may reciprocally influence microbial communities {Bennett, 2001; Certini, 2004; Rogers, 2004; Gleeson, 2005; Gleeson, 2006; Mitchell, 2013; Uroz, 2012; Wild, 2018}. Minerals can thus constitute an ecological niche called the mineralosphere (Uroz et al., 2015). However, factors controlling the interplay between microbial composition and mineral weathering in natural settings remain poorly known.

In this context, the purpose of this study was to evaluate *in-situ* mineral dissolution rates in key compartments of the CZ, to assess the physicochemical parameters controlling the dissolution process and to evaluate its impact on bacterial communities. We incubated *in-situ* fresh mineral powders and polished surfaces (i.e., prepared in the laboratory) directly in environmental settings. This approach attempts to bridge field and laboratory estimates by probing *in-situ* (or “on site”) field weathering rates, and by integrating all biotic and abiotic factors contributing to silicate mineral weathering in the field. Mineral dissolution rates and bacterial communities associated to different types of silicates (see Section 2.1) were directly probed in different compartments of the Strengbach Critical Zone Observatory (CZO, Eastern France). Targeted compartments included (i) rocks in open-air weathering conditions (i.e., direct exposure to meteoric fluids), (ii) two contrasted soil compartments (A and C soil horizons), and (iii) the Strengbach stream at the outlet of the watershed. Direct field estimates of mineral weathering rates were compared to rates predicted with the WITCH model (Godderis et al., 2006) relying on dissolution rate laws derived from laboratory measurements. This enabled to identify factors contributing to the field-laboratory discrepancy. In parallel, bacterial 16S rRNA gene surveys were conducted using high-throughput sequencing to explore the diversity of bacterial communities associated to weathered minerals. Amongst all possible actors of microbial weathering, we focus here on bacteria, whose role in mineral weathering have already been extensively described in literature (see e.g. Uroz et al., 2015 for a review).

## 2. METHODS

### 2.1. Mineral selection

Labradorite, olivine and quartz were selected for this study as model minerals. Labradorite is a tectosilicate belonging to the plagioclase feldspar series, which prevails in the continental crust. Labradorite is a rather reactive feldspar with a composition approximately halfway between albite and anorthite end-members. It contains Na, Ca and some K cations, whose pools may be threatened by some forestry practices in temperate forest ecosystems (Lucas et al., 2011; van der Heijden et al., 2013; Johnson et al., 2015). The labradorite used in this study originates from Madagascar and has the following average composition:  $\text{Na}_{0.5}\text{Ca}_{0.5}\text{Al}_{1.5}\text{Si}_{2.5}\text{O}_8$  (Wild et al., 2016). The olivine used here originates from San Carlos and has a composition close to the pure forsterite pole ( $\text{Fo}_{92.0\pm 1.3}$ ), as determined by inductively coupled plasma atomic emission spectroscopy (ICP-AES) after a standard lithium metaborate fusion. Olivine is a nesosilicate that is characteristic of mafic to ultramafic geological settings. While this mineral is exogenous to the geological context of the study site, it contains Fe and Mg, which are relevant micronutrients in forest ecosystems, and especially for the Strengbach catchment. Fe is a limiting nutrient in most aerobic natural settings (Johnstone and Nolan, 2015) due to rapid Fe oxidation kinetics (Davison and Seed, 1983) and low bioavailability (Saha et al., 2013). Deficiency in bioavailable Mg has been reported for the Strengbach CZ (Bonneau et al., 1991; Dambrine et al., 1992). Quartz was provided by the Museum of Mineralogy of Strasbourg (France). Quartz is nutrient-free, and it was used in parallel as a non-weatherable reference under the reacting conditions and over the time scales considered (Knauss and Wolery, 1988; Tester et al., 1994).

### 2.2. Study site

Mineral samples were incubated at the Strengbach catchment (Observatoire Hydrogéochimique de l'Environnement, Alsace, France; 48°12'48.33"N; 7°12'2.23"E, 1146 m (summit) to 883 m (outlet)), involved in the French and international critical zone observatories network (OZCAR, <http://www.ozcar-ri.org/>; RBV, <http://portail-rbv.sedoo.fr/?locale=en#CMSConsultPlace:HOME>; CZEN, <http://www.czen.org/content/strengbach-catchment-ohge>). The Strengbach stream drains a surface area of 80 ha (Fig. 1A). Forested land comprises 80 % of conifers (*Picea abies*), and 20% of deciduous trees, dominated by *Fagus sylvatica* spp.

The watershed lies on a granitic bedrock, mainly composed of a Hercynian base-poor granite (cordieritic granite) with low Ca and Mg contents, which has been strongly hydrothermally altered on the northern slope and comparatively weakly altered on the southern slope. The top of the northern slope is covered by a 20 to 30 m -thick gneiss layer. Several microgranite intrusions occurred in the southern face (El Gh'Mari, 1995; Pierret et al., 2014).

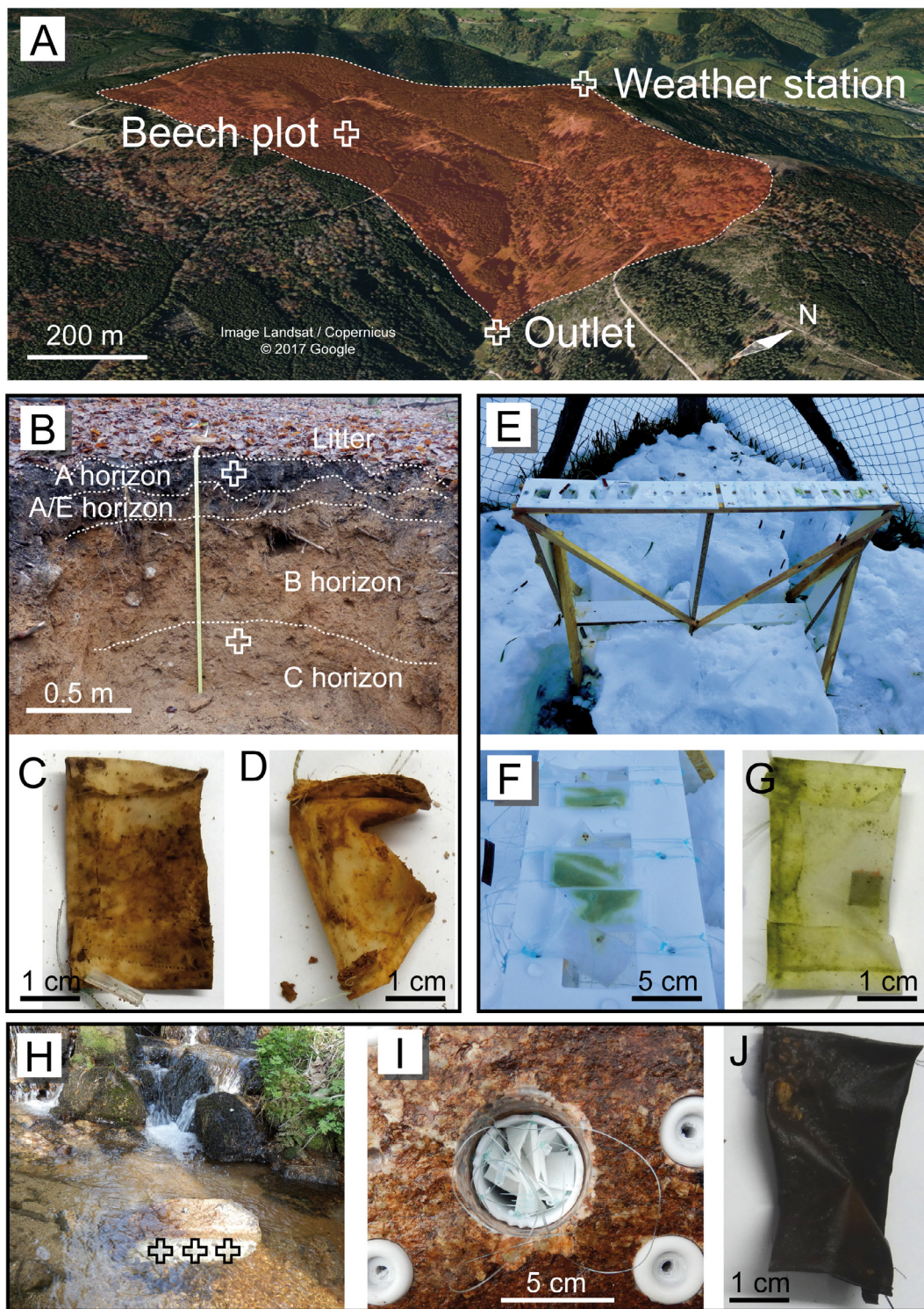


Fig. 1. Compartments of the critical zone probed at the Strengbach catchment (A). Soil profile of the beech plot (B) and corresponding reactivity probes after 20 months of incubation in the A horizon (C) and the C horizon (D). Overview of the setup for sample exposure to atmospheric weathering (E) onto a Polytetrafluoroethylene (PTFE) plate (F). Reactivity probe after 20 months of incubation at the weather station (G). Experimental setup used to immerse samples into the Strengbach stream at the outlet (H) with flow-through PTFE holders (I). Reactivity probe after 20 months of incubation into the Strengbach stream (J). White and black crosses indicate sample locations.

The soils of the watershed range from ochre podzolic soils to brown acidic soils (Lefèvre, 1988). Since 1985, the OHGE is equipped for continuous monitoring of climatic and hydrogeochemical parameters (Viville et al., 2012; Pierret et al., 2014). Climatic data were obtained from a weather station (Fig. 1 A).

The pedological parameters of 10 soil samples collected at the beech plot on 11/18/2013 and 12/02/2014 were analyzed at INRA, Arras, France (Tables A.1–A.4; Fig. 1B). About 1 kg of soil samples was collected at several depths along a 120 cm depth soil profile. Water content was estimated by weighing samples before and after drying at 110 °C. Soil samples were quartered and sieved (2 mm) as described in previous studies (Lucas et al., 2011; Duplay et al., 2014). Granulometry and organic fractions were determined according to SOL-0303 and SOL-0401 standardized procedures, respectively.

### 2.3. Experimental setting

Two sets of mineral probes were incubated simultaneously into four contrasted compartments of the CZ (atmosphere, A and C soil horizons and stream). The mineral probes were collected separately after 9 and 20 months to evaluate temporal changes. Each set of probes consisted of two types of probes: (i) integrative reactivity probes to estimate *in-situ* mineral dissolution rates, and (ii) environmental probes to characterize bacterial communities associated to each mineral type.

#### 2.3.1. Integrative reactivity probes

The integrative reactivity probes consisted of fresh mineral surfaces of labradorite and olivine prepared by polishing raw materials to eliminate the impact of surface ageing on surface reactivity. A Room Temperature Vulcanizing (RTV) glue mask was deposited on each polished surface to enable direct measurements of the mean mineral weathering rates *in-situ*, integrated over the incubation time, by comparing the topography of the mineral sample before and after incubation (Wild et al., 2016; see also Section 2.4). The reactivity of samples is quantified by surface-normalized dissolution rates ( $\text{mol}\cdot\text{m}^{-2}\cdot\text{s}^{-1}$ ) throughout this article.

Samples were cleaned with ethanol and packed into 100  $\mu\text{m}$ -calibrated mesh nylon cloth (Fisher Scientific, Pittsburgh, PA) to allow circulation of soil fluids and microorganisms. Each nylon bag was individually sealed by sewing with 0.12 mm nylon thread. Bags were sterilized, and DNA was eliminated under UV light and rinsed with 0.2- $\mu\text{m}$  filtrated ethanol. Bags were then dried under laminar flow and kept sterile until incubation at the Strengbach catchment (see Fig. 1-A, and Section 2.3.3).

#### 2.3.2. Environmental probes

The environmental probes consisted of nylon bags filled up with sterile labradorite, olivine and quartz powders for bacterial colonization. Powder preparation and sterilization was performed as described in Wild et al. (2016) and Wild et al. (2018). Briefly, olivine, labradorite and quartz crystals were crushed with a hydraulic press, and the pow-

der was dry sieved to recover the 160–315  $\mu\text{m}$  fraction (Fig. A.1). Residual fine particles were removed by successive sonication steps in ethanol. The removal of particles was assessed by SEM observations. The specific surface area of powders was measured using the Brunauer-Emmet-Teller method (BET, Brunauer et al., 1938). Powders were washed for 10 minutes in sterile vessels with two successive baths of 0.2  $\mu\text{m}$  filtered absolute ethanol, dried for > 60 min under sterile laminar flow and exposed to ultraviolet radiation for 20 min. A known amount of powder (2.5–3.5 g) was then sealed in a nylon bag allowing circulation of environmental fluid and microorganisms. Environmental probes were further cleaned and sterilized prior to their incubation at the Strengbach catchment as described previously. Empty control bags were added to each set to evaluate the effect of the nylon bag on bacterial communities.

#### 2.3.3. Incubation of the probes in CZ compartments

A first set of probes was fixed to a perforated Polytetrafluoroethylene (PTFE) plate allowing rainfall to flow across the nylon bags (Fig. 1E and F). Probes were placed at the weather station (Fig. 1A; 48°13'0.56"N; 7°11'47.82" E). Samples were directly exposed to atmospheric weathering (wind, rainfall and meteoric deposits). This “meteoric” compartment represents the entry point at the atmosphere-soil interface of the CZ, which is not influenced by soil hydrological or pedogenesis processes.

Two other sets of probes were incubated into the A-horizon (10-cm depth) and the C-horizon (>60 cm) of the soil profile (Fig. 1B) of the reference beech plot (48°12'41.04"N; 7°11'45.66"E). This plot was selected as it combines higher rainfall volumes (northern slope), simple topography (single slope, Fig. 1A) and homogeneous soil and forest covers. Incubation depths corresponded to that of zero-tension lysimetric plates collecting soil solutions since 1992. Mean pH of solutions from A-horizon was  $4.22 \pm 0.17$  (1992–2016 period,  $n = 178$  measurements). In the C horizon, a lower dissolution rate is expected due to higher pH values (mean  $\pm$  SD:  $4.89 \pm 0.28$ ; 1992–2016 period,  $n = 104$  measurements). Overall, hydrological, geochemical and microbial processes at the A-horizon (topsoil, leaf litter) and the C-horizon (saprolite) are expected to differ.

The fourth set was incubated in the Strengbach stream, at the outlet of the watershed (48°13'0.56"N; 7°12'20.95"E), to allow for a permanent fluid-mineral contact. Samples were inserted into PTFE tubes and oriented in the stream flow direction (Fig. 1H and I). The average pH of the stream measured at the outlet was  $6.46 \pm 0.24$  for the period of incubation (2014/2015).

The sets of probes were collected separately after 9 months (from March 3rd, 2014 to December 2nd, 2014) and 20 months (from March 3rd, 2014 to November 9th, 2015) using sterile forceps. The probes were individually placed into sterile 50 mL Falcon tubes and transported into the laboratory in a sealed cooler and further handled under sterile laminar flow. Probes were collected during the same season (fall) to limit seasonal effects on microbial communities of the mineralosphere (Collignon et al., 2011).

## 2.4. Measurement of mineral weathering rates

Vertical scanning interferometry (VSI, Zygo New View 7300) was used to estimate mineral weathering rates  $r$ , based on the global retreat ( $\Delta z$ ) of the surface of each integrative reactivity probe after incubation, compared to an unreacted (masked) portion of the same mineral surface, as follows:

$$r = \frac{\Delta z}{\Delta t * V_m} \quad (1)$$

where  $\Delta t$  stands for the incubation duration and  $V_m$  is the molar volume of the considered mineral. This approach was previously shown to provide dissolution rates consistent with classical powder dissolution experiments (Arvidson et al., 2003; Arvidson and Lutge, 2010; Daval et al., 2013), and has been applied here for the first time in the field.

## 2.5. Predictions of mineral weathering rates

The WITCH model (Godderis et al., 2006) was used to evaluate mineral dissolution rates of samples in soil. The model used physicochemical parameters recorded *in-situ* during mineral incubation. WITCH reproduces *in-situ* reactivity conditions (e.g. parameters of the reactive fluids including T, pH and more generally, solution composition) at stake during probe incubation using the OHGE database (1987–2016). Modeled mineral dissolution rates relying on kinetic rate laws derived from previous laboratory weathering experiments were compared to *in-situ* measurements based on integrative reactivity probes (field rates). Input parameters of WITCH model such as the solubility products of secondary phases were previously adjusted in various contexts (Beaulieu et al., 2012; Beaulieu et al., 2010; Godderis et al., 2006; Violette et al., 2010). Therefore, differences between modeled and observed dissolution rates were interpreted here in terms of field-lab discrepancy.

Briefly, the model considered a one-dimensional soil profile discretized into 36 homogeneous boxes of 5-cm height overlying a bedrock layer. At each time step, the code solves the following mass-balance equation for each box:

$$\frac{dC}{dt} = F_{up} - F_{down} + F_{weath} - F_{prec} + F_{ex} + F_{veg} \quad (2)$$

where  $C$  is the concentration of a given dissolved species in the considered box.  $F_{up}$  represents the input flux at the top of the considered box through drainage while  $F_{down}$  is the output flow through downward drainage.  $F_{weath}$  and  $F_{prec}$  stand for the release of a given species from primary minerals through weathering processes or for its consumption by the precipitation of secondary phases, respectively.  $F_{ex}$  and  $F_{veg}$  stand for the fluxes associated to the exchange of this species with the argilo-humic complex or with the vegetation (either nutrient consumption or organic matter decay), respectively. Input fluxes were estimated by a series of rain gauges and an experimental setup at the beech plot dedicated to throughfall and soil solution collection (Prunier et al., 2015, <http://ohge.unistra.fr/>). Output elemental

fluxes from the watershed were quantified by an experimental hut located at the catchment outlet, where water discharge, solute concentrations, suspended matter and sediments are continuously quantified (Viville et al., 2012). Fluxes related to mineral weathering were calculated as follows:

$$F_{weath} = Area_{Min} * \phi_{Min} * SMS * x_{molar} * R_{min} \quad (3)$$

where  $Area_{Min}$  corresponds to the mineral specific surface area in  $m^2_{mineral} \cdot m^{-3}_{soil}$ ,  $\phi_{Min}$  stands for the volumetric proportion of that mineral in the considered soil horizon,  $x_{molar}$  is the stoichiometric coefficient of the element of interest in the considered mineral.  $SMS$  refers to the soil moisture saturation (Sverdrup, 1990; Warfvinge and Sverdrup, 1992; Sverdrup and Warfvinge, 1993):

$$SMS = \frac{\theta * \rho_{solid}}{\rho_{solid} - \rho_i + \theta * \rho_{water}} \quad (4)$$

where  $\rho_{solid}$  and  $\rho_{water}$  are the density of the soil particles and water respectively ( $kg \cdot m^{-3}$ ),  $\rho_i$  is the bulk density of the soil and  $\theta$  is the dimensionless soil water content. The water content of each soil layer and the vertical drainage used by the WITCH model were estimated using the BILJOU© model (Granier et al., 1999).

$R_{min}$  ( $mol \cdot m^{-2} \cdot s^{-1}$ ) is the mineral weathering rate defined as:

$$R_{min} = \left[ \sum_i A_{i,min} \cdot \exp\left(\frac{-E_{a,min}^i}{RT}\right) \cdot a_i^{n_{i,min}} \right] (1 - \Omega^S) \quad (5)$$

where  $A_{i,min}$  ( $mol \cdot m^{-2} \cdot s^{-1}$ ) is the Arrhenius pre-exponential factor,  $R$  ( $J \cdot mol^{-1} \cdot K^{-1}$ ) the gas constant and  $T$  ( $K$ ) the absolute temperature, respectively.  $E_{a,min}^i$  ( $J \cdot mol^{-1}$ ) is the activation energy,  $a_i$  the dimensionless ion activity and  $n_{i,min}$  the dimensionless reaction order with respect to the hydrolysis of mineral  $min$  by the reactive species  $i$  (either  $H^+$ ,  $OH^-$ ,  $H_2O$  or an organic ligand).  $\Omega$  is the dimensionless mineral saturation index and  $S$  is a dimensionless empirical fitting parameter (Maher et al., 2009) assimilated to a “stoichiometric number” (Godderis et al., 2006; Godd ris and Donnadieu, 2009) equal to 1 for olivine and to 1/3 for labradorite according to the WITCH database.

The soil mineral specific surface area was estimated from soil texture according to a parametric law (Sverdrup and Warfvinge, 1995):

$$Area_{Min} = \rho * (8.0 * X_{clay} + 2.2 * X_{silt} + 0.3 * X_{sand}) \quad (6)$$

where  $\rho$  is the density of the considered soil layer, and  $X_{clay}$ ,  $X_{silt}$ , and  $X_{sand}$  correspond to the clay, silt and sand fraction, respectively, with

$$X_{clay} + X_{silt} + X_{sand} = 1 \quad (7)$$

Soil texture (different fractions), density and porosity were measured on-site for the superficial and the deep layers (5- and 150 cm-depth respectively). The average composition of top and deep soil layers considered to run simulations were: 15% clay, 19% silt and 66% sand, and 9% clays, 19% silt and 72% sand, respectively (according

to Table A.2 and Beaulieu et al., 2016). The mineralogical composition in each box was calculated by linear interpolation of measured data given above. The relative proportions of olivine and labradorite ( $\phi_{\text{olivine}}$  and  $\phi_{\text{Labradorite}}$ ) were set to 0.001% to make sure that their contribution to the modeled solution composition remains negligible. The flux of exchangeable ions ( $Ca^{2+}$ ,  $Mg^{2+}$ ,  $K^+$ ,  $SO_4^{2-}$ ,  $HPO_4^{2-}$ ,  $Al^{3+}$  et  $Na^+$ ) was defined following a Fickian diffusion law:

$$\frac{dE_{EC}}{dt} = -k_x(EC_{surf} - EC_{sol}) \quad (8)$$

where  $E_{EC}$  is the fraction of sites occupied by an exchangeable ion  $EC$ , and  $k_x$  is a mass transfer coefficient determined according to the literature (Warfvinge and Sverdrup, 1988).  $EC_{sol}$  and  $EC_{surf}$  are concentrations calculated in the bulk solution and at the surface of the argilo-humic complex, respectively, based on data from the literature (Alveteg, 1998). Element exchanges between vegetation and soil ( $F_{veg}$ ) were estimated based on carbon net primary production and carbon recycling determined by the Lund-Potsdam-Jena (LPJ) dynamic global vegetation model (Sitch et al., 2003), and from element/carbon ratios established by Redfield (see Drever et al., 1997). Plant nutrient uptake was allowed down to 1.5 m depth (root compartment), whereas elemental release from litter degradation was only allowed in the superficial soil horizon (above 0.5 m depth) (Beaulieu et al., 2010; Roelandt et al., 2010; Beaulieu et al., 2012). Soil acidification from carbon dioxide partial pressure ( $p_{CO_2}$ ) induced by autotrophic and heterotrophic respirations were calculated from climatic data (precipitation, temperature, cloud cover, atmospheric  $CO_2$  concentration) sourced from the OHGE and CRU-TS global databases (Harris et al., 2014). The actual chemical composition of input solutions (throughfall) as a boundary condition at the top of the soil column at each time step was determined using the dynamic version of the code. The model was calibrated using time series from 1987 to 2015 and comparison of the composition of soil solutions collected from the lysimetric plates with those predicted at the corresponding depth (see Tables A.5 and A.6). Sulfate concentration, which only depends on hydrological parameters due to the absence of weatherable sulfate-bearing phases at the Strengbach watershed, were reproduced for the A-horizon (Table A.5). The temperature profile along the soil column was defined for each box by linear interpolation between surface temperature and temperature at 1.5 m-depth, defined at each time step as the gliding annual mean of surface temperatures.

For mineral samples immersed in the Strengbach stream and at the weather station, predicted surface retreats were estimated assuming permanent contact of the mineral with a solution at a pH corresponding to annual average pH of the stream or of the rainfall, respectively. The solution-mineral interaction was assumed to be constant throughout the incubation period at a temperature corresponding to the annual mean water and air temperature, respectively.

## 2.6. Bacterial community analysis

### 2.6.1. DNA extraction

Total DNA was extracted from the soil samples and the stream sediments with a PowerSoil® DNA Isolation Kit (MO BIO, Carlsbad, CA, USA) following manufacturer's instructions. DNA extraction were performed on single samples due to limited quantities of incubated powder. The concentrations of DNA were determined using a Qubit® Fluorometer and Qubit® dsDNA HS Assay Kit (Invitrogen, Carlsbad, CA, USA). A DNA extraction was first carried out from sterile mineral powder before incubation in the CZ compartment. DNA could not be detected in sterile and cleaned samples. Concentrations of DNA extracted from incubated probes ranged from 0.1 to 2.1 ng· $\mu\text{L}^{-1}$  for atmospheric probes, 0.6 to >6 ng· $\mu\text{L}^{-1}$  for A-horizon probes, 0.1 to >6 ng· $\mu\text{L}^{-1}$  for C-horizon probes, and 3.69 to >6 ng· $\mu\text{L}^{-1}$  for stream probes.

### 2.6.2. Illumina MiSeq sequencing and data processing

The sequencing procedure has been described previously (Babcsanyi et al., 2017). Sequencing was performed at the Research and Testing Laboratory (Lubbock, TX, USA) using Illumina MiSeq. The 16S rRNA gene spanning hypervariable region V4 was amplified in a two-step process. Forward primer was based on illumina i5 primer (5'-TCGTCGGCAGCGTCAGATGTGTATAAGAGACAG-3') the universal bacterial 515F primer (5'-GTGCCAGC MGCCGCGGTAA-3') (Walters et al., 2011). Corresponding reverse primer was synthesized from illumina i7 primer (5'-GTCTCGTGGGCTCGGAGATGTGTATAAGAGACAG-3') and universal bacterial primer 806R (5'-GGAC TACHVGGGTWTCTAAT-3'). Sequences were generated by nested polymerase chain reaction (PCR) in 25  $\mu\text{L}$  reactors filled up with 1  $\mu\text{L}$  of 5  $\mu\text{M}$  primer solution and 1  $\mu\text{L}$  of DNA matrix, diluted in a nucleotide-Taq polymerase-MgCl<sub>2</sub> mix. (Qiagen HoStar Taq master mix, Qiagen Inc., Valencia, CA). Reaction was performed in an ABI Veriti incubator (Applied Biosystems, Carlsbad, CA). Reaction products were reamplified by a second PCR step. Primers used in this second step were based on Illumina Nextera sequences:

AATGATACGGCGACCACCGAGATCTACAC[i5index]TCGTCGGCAGCGT for the forward and -CAAGCA GAAGACGGCATAACGAGAT[i7index]GTCTCGTGGGCTCGG for the reverse. Generated amplicons were visualized with eGels (Life Technology, Grand Island, NY). Products were divided into several equimolar samples and sorted according to their size by Agencourt AMPure XP (Beckman Coulter, Indianapolis, IN) on a 0.7 ratio basis for each step. DNA concentrations were determined with a Qubit 2.0 spectrofluorometer (Life Technologies, Grand Island, NY) and samples were then loaded in an Illumina MiSeq sequencing device (Illumina Inc., San Diego, CA), equipped with two fluid cells. The data have been deposited with links to BioProject accession number PRJNA492367.

Denosing, chimera checking, generation of operational taxonomic units (OTUs) and taxonomic classification were performed using the custom-scripted bioinformatics pipeline of the Research and Testing Laboratory (Lubbock,



TX, USA). Based on the sequence identity percentage derived from BLASTn (Altschul et al., 1990), sequences with identity scores to known or well-characterized 16S rRNA gene sequences >97% identity (<3% divergence) were resolved at the species level, >95% to 97% at the genus level, >90% to 95% at the family level, >80% to 90% at the order level, >80 to 85% at the class level and between 77% and 80% at the phylum level. Any match below this identity level was not used in taxonomical analysis. Matrices of taxonomic data were further used to visualize changes in community composition.

### 2.6.3. Bacterial diversity and composition analysis

Principal Coordinate Analyses (PCoA) based on Bray-Curtis dissimilarities (Bray and Curtis, 1957; Odum, 1950) was used to visualize ecological gradients underlying the composition of bacterial communities of the environmental probes. PCoA were performed on R software with the *vegdist* function of the *vegan* package (Oksanen et al., 2013). The relationship between community profiles and the proportion of phylotypes in each sample was investigated by *a posteriori* projection of the genera as weighed average of their contribution to the samples onto the PCoA biplot. Discontinuities within the dataset were revealed by applying a Ward hierarchical clustering (Ward, 1963) as an aggregation rule on Bray-Curtis dissimilarities (Bray and Curtis, 1957; Odum, 1950) with the *hclust* function of the *stats* package. Analysis of similarities (ANOSIM) was used to infer statistical differences between bacterial community clusters ( $P < 0.01$ ) whenever possible. Final clusters were selected on the basis of the corresponding average silhouette width. The significance of the axes in each biplot representation was evaluated following Kaiser-Guttman criterion.

To calculate the diversity and richness indices, the Illumina MiSeq sequences were re-analyzed using MOTHUR version 1.36.1 (<http://www.mothur.org>) starting from denoised and chimera-checked sequences, aligned, and clustered to define OTUs at 97% sequence identity. Two equiv-

alent datasets were then randomly sub-sampled according to the procedure developed by Schloss et al. (2009). The resulting datasets were used for rarefaction analysis and to calculate the diversity and richness indices (i.e., Shannon diversity index ( $H'$ ), inverse Simpson diversity and Chao 1 richness index (Schao1), Babcsanyi et al., 2017).

## 3. RESULTS

### 3.1. Soil nutrient pool

Soil physicochemical parameters are provided in Tables A.1–A.4. The profiles of Mg and Ca cationic exchange capacities as a function of depth, which corresponds to inorganic nutrients of interest in the present study, are shown in Fig. 2.

### 3.2. In-situ mineral dissolution rates

Topography measurements on crystals incubated at the Strengbach catchment for 9 and 20 months enabled to estimate the maximal dissolution rates based on surface retreats or roughness (Tables 1 and 2). The surface retreats for olivine ranged from 1 nm ( $9.38 \times 10^{-13} \text{ mol}\cdot\text{m}^{-2}\cdot\text{s}^{-1}$ ) to 171 nm ( $7.17 \times 10^{-11} \text{ mol}\cdot\text{m}^{-2}\cdot\text{s}^{-1}$ ), both obtained from the meteoric sets of probes (at the weather station). Overall, upper boundaries of reaction rates for olivine were  $3.63 \times 10^{-11} \text{ mol}\cdot\text{m}^{-2}\cdot\text{s}^{-1}$  (meteoric),  $1.20 \times 10^{-11} \text{ mol}\cdot\text{m}^{-2}\cdot\text{s}^{-1}$  (soil A horizon),  $1.12 \times 10^{-12} \text{ mol}\cdot\text{m}^{-2}\cdot\text{s}^{-1}$  (soil C horizon) and  $1.70 \times 10^{-12} \text{ mol}\cdot\text{m}^{-2}\cdot\text{s}^{-1}$  (stream).

For labradorite, surface retreats ranged between 1 nm (stream, C horizon) and 5 nm (stream), corresponding to reaction rates ranging from  $1.92 \times 10^{-13}$  to  $2.15 \times 10^{-12} \text{ mol}\cdot\text{m}^{-2}\cdot\text{s}^{-1}$ . The average upper boundaries of reaction rates for labradorite were  $6.21 \times 10^{-13} \text{ mol}\cdot\text{m}^{-2}\cdot\text{s}^{-1}$  (meteoric),  $1.02 \times 10^{-12} \text{ mol}\cdot\text{m}^{-2}\cdot\text{s}^{-1}$  (A horizon),  $6.20 \times 10^{-13} \text{ mol}\cdot\text{m}^{-2}\cdot\text{s}^{-1}$  (C horizon) and  $1.37 \times 10^{-12} \text{ mol}\cdot\text{m}^{-2}\cdot\text{s}^{-1}$  (stream). Of note, Daval et al.

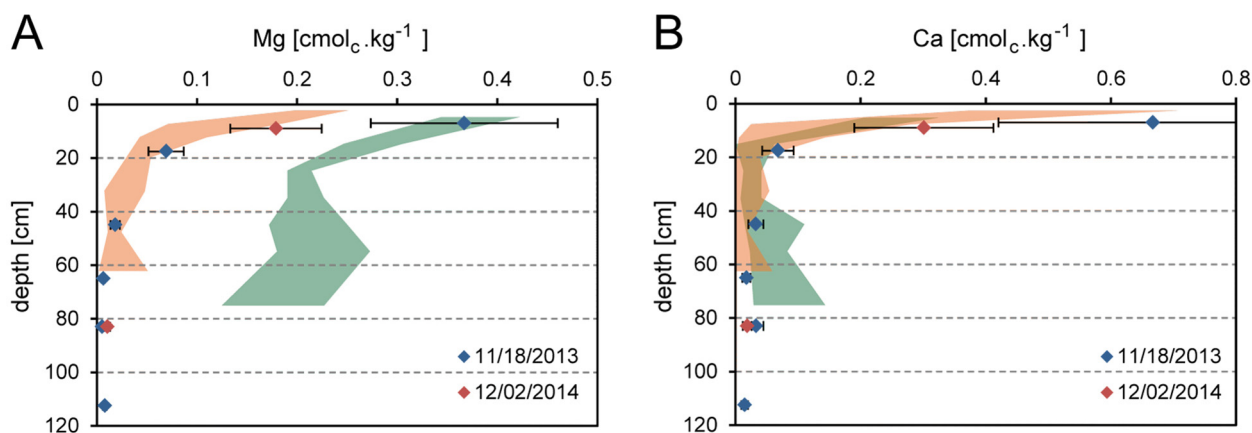


Fig. 2. Exchangeable Mg (A) and Ca (B) determined by ammonium acetate extractions on samples of the soil profile of the beech plot collected on 11/18/2013 and 12/02/2014 (see Table A.3). For comparison, green and orange plots represent corresponding concentrations measured at the experimental plot of Breuil-Chenu (Morvan, France) before and 30 years after deforestation respectively (van der Heijden et al., 2013).

Table 1

Global retreat of the surface of labradorite  $\Delta_z$  and associated dissolution rate  $r$  measured *in-situ* in the field ( $F$ ) or issued from WITCH simulations from kinetic rate laws determined in the laboratory ( $L$ ), based on the transition state theory. Values between parentheses are based on a rate -  $\Delta G_r$  relationship by Taylor et al. (2000). Predicted extent of reaction  $\xi$  and associated field-laboratory discrepancies  $\Delta_{L/F}$ . n.d. could not be estimated based on the methodology proposed here, since expected retreats were lower than uncertainties due to the quality of the polishing of the corresponding samples.

| Labradorite |                 |                              |                   |   |        |     |                   |   |                              |                |  |
|-------------|-----------------|------------------------------|-------------------|---|--------|-----|-------------------|---|------------------------------|----------------|--|
| Sample      | Context         | Incubation duration [months] | $\Delta_z^F$ [nm] | $r_F$ [mol·m <sup>-2</sup> ·s <sup>-1</sup> ] | T [°C] | pH  | $\Delta_z^L$ [nm] | $r_L$ [mol·m <sup>-2</sup> ·s <sup>-1</sup> ] | $\xi$ [mol·m <sup>-2</sup> ] | $\Delta_{L/F}$ |  |
| ML9         | Weather Station | 9                            | 2*                | 8.59E-13                                      | 7.1    | 5.4 | 4.4               | 1.88E-12                                      | 4.49E-05                     | 2.2            |  |
| ML20        | Weather Station | 20                           | 2*                | 3.84E-13                                      | 7.1    | 5.4 | 9.8               | 1.88E-12                                      | 1.01E-04                     | 4.9            |  |
| AL9a        | A horizon       | 9                            | 2*                | 8.59E-13                                      | 6.1    | 4.2 | 30.6              | 1.31E-11                                      | 2.93E-04                     | 15.3           |  |
| AL9b        | A horizon       | 9                            | 4.5               | 1.99E-12                                      | 6.1    | 4.2 | 30.3              | 1.34E-11                                      | 2.87E-04                     | 6.7            |  |
| AL20        | A horizon       | 20                           | 1.1*              | 2.11E-13                                      | 6.1    | 4.2 | 59.4              | 1.14E-11                                      | 5.68E-04                     | 54.0           |  |
| CL9a        | C horizon       | 9                            | 1.5*              | 6.44E-13                                      | 6.1    | 5.2 | 6.2 (1.7)         | 2.68E-12 (7.24E-13)                           | 3.26E-05                     | 4.1 (1.1)      |  |
| CL9b        | C horizon       | 9                            | 1*                | 4.42E-13                                      | 6.1    | 5.2 | 6.1 (1.6)         | 2.72E-12 (7.24E-13)                           | 3.16E-05                     | 6.1 (1.6)      |  |
| CL9c        | C horizon       | 9                            | 2.5*              | 1.11E-12                                      | 6.1    | 5.2 | 6.1 (1.6)         | 2.72E-12 (7.24E-13)                           | 3.16E-05                     | 2.4 (0.7)      |  |
| CL20        | C horizon       | 20                           | 1.5*              | 2.88E-13                                      | 6.1    | 5.2 | 11.2 (3.1)        | 2.17E-12 (5.85E-13)                           | 5.95E-05                     | 7.5 (2.0)      |  |
| EL9a        | Stream          | 9                            | 5*                | 2.15E-12                                      | 5.8    | 6.5 | 0.8               | 3.55E-13                                      | 8.45E-06                     | n.d.           |  |
| EL9b        | Stream          | 9                            | 4*                | 1.77E-12                                      | 5.8    | 6.5 | 0.8               | 3.55E-13                                      | 8.21E-06                     | n.d.           |  |
| EL20        | Stream          | 20                           | 1*                | 1.92E-13                                      | 5.8    | 6.5 | 1.8               | 3.55E-13                                      | 1.89E-05                     | 1.8            |  |

Table 2

Global retreat of the surface of olivine  $\Delta_z$  and associated dissolution rate  $r$  measured *in-situ* in the field ( $F$ ) or issued from WITCH simulations from kinetic rate laws determined in the laboratory ( $L$ ), based on the transition state theory. Predicted extent of reaction  $\xi$  and associated field-laboratory discrepancies  $\Delta_{L/F}$ . \*retreat determined on a zone with no specific feature of fluid circulation. \*\*possibly of biotic origin (refer to the text).

| Olivine |                 |                              |                   |   |        |     |                   |   |                              |                |  |
|---------|-----------------|------------------------------|-------------------|---|--------|-----|-------------------|---|------------------------------|----------------|--|
| Sample  | Context         | Incubation duration [months] | $\Delta_z^F$ [nm] | $r_F$ [mol·m <sup>-2</sup> ·s <sup>-1</sup> ] | T [°C] | pH  | $\Delta_z^L$ [nm] | $r_L$ [mol·m <sup>-2</sup> ·s <sup>-1</sup> ] | $\xi$ [mol·m <sup>-2</sup> ] | $\Delta_{L/F}$ |  |
| MO9     | Weather Station | 9                            | 1*                | 9.38E-13                                      | 7.1    | 5.4 | 83.8              | 7.87E-11                                      | 1.70E-03                     | 84             |  |
| MO20    | Weather Station | 20                           | 171               | 7.17E-11                                      | 7.1    | 5.4 | 187.7             | 7.87E-11                                      | 3.82E-03                     | 1              |  |
| AO9     | A horizon       | 9                            | 24.19             | 2.27E-11                                      | 6.1    | 4.2 | 407.2             | 3.82E-10                                      | 8.53E-03                     | 17             |  |
| AO20    | A horizon       | 20                           | 3**               | 1.26E-12                                      | 6.1    | 4.2 | 809.6             | 3.39E-10                                      | 1.71E-02                     | 270            |  |
| CO9     | C horizon       | 9                            | 1.5               | 1.41E-12                                      | 6.1    | 5.2 | 112.1             | 1.05E-10                                      | 1.48E-03                     | 75             |  |
| CO20    | C horizon       | 20                           | 2*                | 8.38E-13                                      | 6.1    | 5.2 | 211.1             | 8.85E-11                                      | 2.75E-03                     | 106            |  |
| EO9     | Stream          | 9                            | 2.5               | 2.35E-12                                      | 5.8    | 6.5 | 21.7              | 2.04E-11                                      | 4.53E-04                     | 9              |  |
| EO20    | Stream          | 20                           | 2.5*              | 1.05E-12                                      | 5.8    | 6.5 | 48.6              | 2.04E-11                                      | 1.01E-03                     | 19             |  |

(2018) indicated that the measured dissolution rates in the A horizon for labradorite powders incubated for over four years in the same location from 2004 to 2008 ( $1.9 \times 10^{-12}$  mol·m<sup>-2</sup>·s<sup>-1</sup>) are similar to those reported above. For some samples, the surface retreat varied significantly along the boundary of the masks (Fig. 3). In such cases, zones with the greatest surface retreats may coincide with zones of preferential fluid circulation, as indicated by material fragments including colluvium or soil sediments (Fig. 3A and C (dashed area) and Fig. 4A and C (zone 2)). Surface retreats presented in Tables 1 and 2 correspond to zones of maximal surface retreat on the crystals where fluid circulation could be evidenced, unless otherwise specified. In addition to global surface retreats (e.g. red arrow, Fig. 5C), local dissolution features were detected (e.g. green arrow, Fig. 5C). These non-geometrical “etch pits” were generally randomly aligned and accounted for locally faster dissolution rates (see red color in Fig. 6B, D and E).

### 3.3. Theoretical mineral reactivity

Dissolution rates of olivine and labradorite in the soil profile were primarily controlled by seasonal temperature variations (for both A- and C-horizons, Fig. 7). Simulated pH values of the A horizon ( $4.3 \pm 0.2$ ) was in agreement with observed values ( $4.37 \pm 0.14$ ), whereas simulated values ( $5.4 \pm 0.2$ ) for the C horizon were slightly higher than those observed ( $4.83 \pm 0.07$ ). The simulated solution compositions in the A and C horizons corresponded to far-from-equilibrium conditions with respect to both labradorite and olivine (i.e.,  $\Omega$  values close to 0 in Eq. (5)). Based on the transition state theory used in the WITCH model (Eq. (5)), such undersaturation states corresponded to dissolution rates that were virtually not affected by the chemical affinity of the system.

For samples from the soil profile, predicted dissolution rates converted into global surface retreats were one to two orders of magnitude greater than rates measured

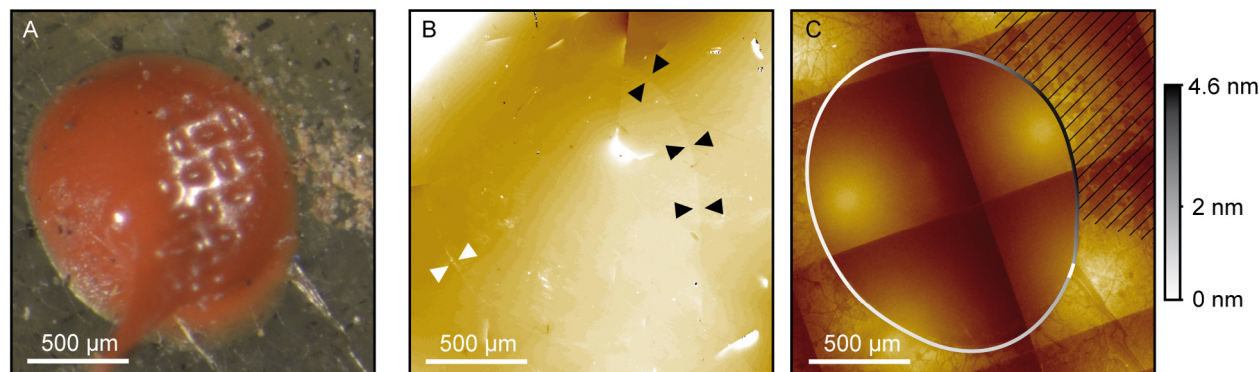


Fig. 3. Labradorite sample collected after 9 months of incubation in the C horizon of the soil profile of the beech plot at the Strengbach catchment. Stereo microscope image acquired before removal of the Room Temperature Vulcanizing (RTV) glue mask (A), vertical scanning interferometry (VSI) surface topography after cleaning (B) and interpretation in terms of surface retreat overlaid on stitched VSI images before removal of the RTV glue mask (visible inside the circled area) of the same portion of the sample (C). Black arrowheads in (B) indicate zones of global surface retreat at the mask location. White arrows indicate another boundary of the mask indicated by a residue of RTV glue. The striped zone in (C) corresponds to a location of possible natural fluid circulation (see text).

*in-situ* for olivine (Table 2). The laboratory-field discrepancy for dissolution rates in the A horizon varied by a factor of 17 to more than 250 for olivine, and from about 7 to more than 50 for labradorite. In the C horizon, the minimum field-laboratory discrepancy was generally weaker, and ranged from 75 to more than 106 for olivine and from 2 to 7.5 for labradorite.

Regarding the set of probes exposed to the atmosphere, the predicted retreat based on the annual average rainfall properties (pH = 5.4; T = 7.1 °C) overestimated the maximal measured retreats by a factor of about 2 for labradorite, and up to a factor of 80 for olivine. Of note, a sample of olivine locally exhibited a retreat of 171 nm, which corresponds to a factor of ~1 (no laboratory-field discrepancy).

For samples incubated in the Strengbach stream, theoretical calculations based on the annual average parameters describing water of the Strengbach stream (pH = 6.5; T = 5.8 °C) overestimated the measured values by a factor of 9 to 19 for olivine, and a factor of  $\geq 1.8$  for labradorite.

### 3.4. Diversification and composition of bacterial communities

#### 3.4.1. General patterns

An average of 33,719 high-quality sequences ( $\sim 250$  bp) were obtained for each sample by Illumina MiSeq after analysis with Mothur. The OTUs covered 29 phyla, 322 families and 722 genera. Although the sequencing depth (see Fig. A.2 for rarefaction curves) did not systematically allow for a survey of the full extent of bacterial diversity, rarefaction curves of diversity indices reached asymptotes (Fig. A.2). This indicates sufficient sampling depth to capture the diversity of bacterial communities.

Bacterial community composition of the soil, the weather station and the stream sets significantly differed ( $P < 0.01$ ), irrespective of the incubation time. Sets incubated at the weather station (Fig. 1G) were the richest in Cyanobacteria (>18%) and in Bacteroidetes (>22%, Fig. 8), whereas those from the soil (Fig. 1C and D) were enriched in Acidobacteria (>20% horizon A, >16%,

horizon C). Samples immersed in the stream (Fig. 1J) exhibited a higher mean abundance of Verrucomicrobia.

Differences between compartments of the CZ were also observed at the genus level, in particular amongst taxa potentially involved in mineral weathering processes. For instance, highest proportions of OTUs corresponding to *Geobacter* sp., typical from sedimentary environments and involved in Fe(III) reduction through anaerobic respiration (Esther et al., 2015), were found in the outlet samples. *Aquabacterium* sp. or *Rhodobacter* sp., which encompass several species known for their iron oxidizing capabilities (Hedrich et al., 2011; Weber et al., 2006), were only found in significant proportions in the stream set of probes. Genera known for their ability to weather iron-bearing silicates through siderophore production such as *Sphingomonas* sp. (Calvaruso et al., 2007; Uroz et al., 2009, 2007), or identified as dissimilatory iron-reducing bacteria (DIRB), such as *Acidiphilium* sp. (Esther et al., 2015) were exclusively found in significant proportions on samples subjected to atmospheric weathering (i.e., at the weather station), especially on olivine samples. Both extracted DNA amounts and diversity indices were larger for the stream sets compared to the soil sets, and generally lower for the sets exposed to the atmosphere (Fig. A.3).

#### 3.4.2. A- and C-horizons soil sets

Bacterial communities of the A horizon differed significantly from those of the C horizon ( $P < 0.01$ ). Taxa potentially involved in mineral alteration appeared to be unevenly distributed between A and C horizons. For example, phylotype sharing 100% similarity with *Mycobacterium kyorinense* strain KUM 060200 16S ribosomal RNA gene, belonging to the genus *Mycobacterium* associated to biotite alteration within the oak mycorrhizosphere (Uroz et al., 2009), was only found in litter samples in relative abundance exceeding 0.1%.

Clustering of samples from both the A and C horizons emphasized distinct communities for mineral probes or environmental matrices (i.e. soil) (Fig. 9A and C). In the

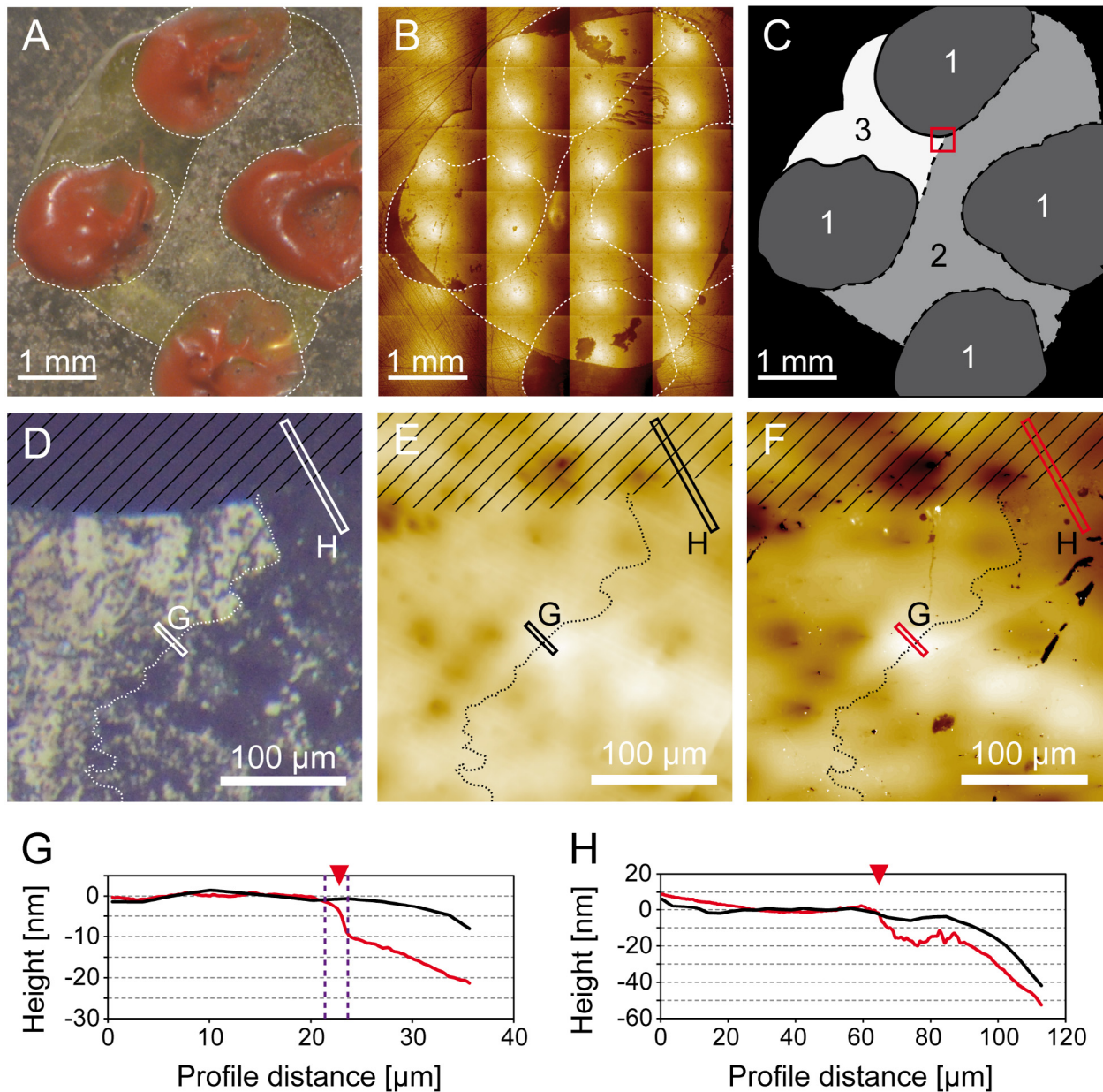


Fig. 4. Olivine samples after 9 months of incubation in the A horizon of the soil profile of the beech plot at the Strengbach catchment. Stereo microscope image acquired before removal of the RTV glue mask (A) and stitched VSI images of the surface after cleaning (B). Dashed lines indicate the boundary of zones interpreted in (C) as portions of masked olivine surface (1), olivine surface including traces of possible fluid circulation (2), or olivine surface exposed to the soil environment (3). Red box in C indicates the portion of the surface imaged by stereo microscope right after incubation (D) or by VSI before (E) and after (F) 9 months of incubation. Striped zone in (D), (E) and (F) correspond to the masked area. Profiles at the boundary between zones 2 and 3 and zones 1 and 2 (indicated by a red arrowhead) before (in blue) and after (in red) 9 months of incubation are reported in (G) and (H) respectively. (For interpretation of the references to colour in this figure legend, the reader is referred to the web version of this article.)

A horizon, bacterial communities from the control empty bags incubated for 9 months, and the quartz samples incubated for 20 months, also differed from the rest of the samples (Fig. 9D). These samples exhibited lower diversity than other samples from the A horizon, as evidenced by their inverse Simpson ( $I$ ) and Shannon ( $H'$ ) diversity indices (Fig. A.3A and B). The richness and bacterial diversity of the olivine sample collected after 20 months of incubation

in the A horizon (O20) were higher than for all other samples of the A horizon (Fig. A.3A and B), and similar to richness and bacterial diversity of corresponding soil sample (Schao1 > 4000; Fig. A.3C).

Regarding the C-horizon, bacterial communities changed according to both incubation time (9-month samples versus 20-month samples, Fig. 9A) and mineral type (Fig. 9A). The bacterial diversity indices associated with

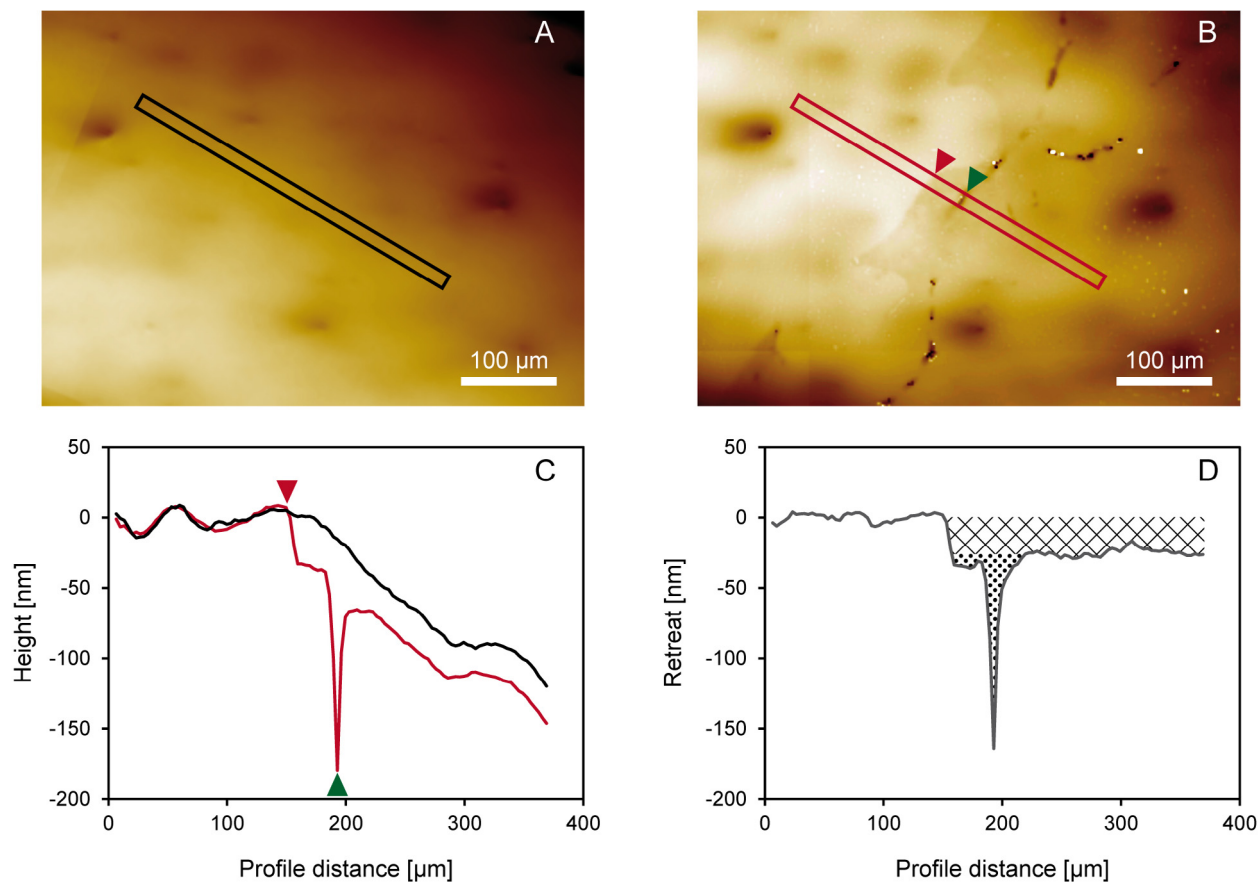


Fig. 5. Surface topography of an olivine reactivity probe before (A) and after (B) 9 months of incubation in the A horizon of the soil profile at the beech plot. Superposition of profiles before (black) and after (red) incubation (C) and corresponding surface retreat (D). Global surface retreat (red arrow, C; dashed area, D) and local alteration features (green arrow, C; dotted area, D). (For interpretation of the references to colour in this figure legend, the reader is referred to the web version of this article.)

labradorite and olivine were the highest ( $H' > 5$  and  $I > 50$ ) after 20 months of incubation, and close to those of soil samples. Although diversity was on average lower after 9 months, bacterial diversity for labradorite and olivine was systematically larger than that for quartz. The bacterial diversity for labradorite was higher than that of olivine and quartz, although the bacterial richness for labradorite differed from that of other C horizon samples (Fig. A.3C).

#### 3.4.3. Weather station

Bacterial communities associated with mineral probes exposed to the atmosphere at the weather station were mainly structured according to the mineral type (Fig. 9A and B). The average bacterial diversity was the lowest among the different sets of this study. The bacterial diversity was the highest for olivine and the lowest for quartz, and significantly increases for olivine between 9 months and 20 months. The olivine sample exhibited the largest specific richness after 20 months of incubation (Shao1 > 2000, Fig. A.3).

#### 3.4.4. Stream sets

Bacterial communities from samples immersed in the Strengbach stream differed from those of the related stream

sediments (Fig. 9G). The difference among mineral probes was lower compared to the difference between mineral probes and the stream sediments. Temporal changes in the bacterial communities were observed (Fig. 9G). The bacterial diversity of environmental probes from the stream was greater than that of probes incubated in other compartments of the CZ ( $H' > 6.9$  and  $I > 400$ , Fig. A.3).

## 4. DISCUSSION

Dissolution rates of fresh minerals, usually obtained from laboratory experiments, generally differ from rates of mineral aged in the field due to changes in the mineral surface chemistry over geologic time scales. In addition, the biogeochemical weathering environment of minerals in the critical zone is still largely unknown. In this study, we incubated in the field mineral samples comparable to those used in laboratory experiments to identify *in-situ* (i) hot-spots of mineral reactivity in the critical zone, (ii) the extent of the field-lab discrepancy, and (iii) main bacterial patterns associated to mineral surfaces. We discuss below the contribution of intrinsic and extrinsic factors to the field-laboratory discrepancy and factors that may be accounted for to limit this discrepancy. Possible effects of bacterial

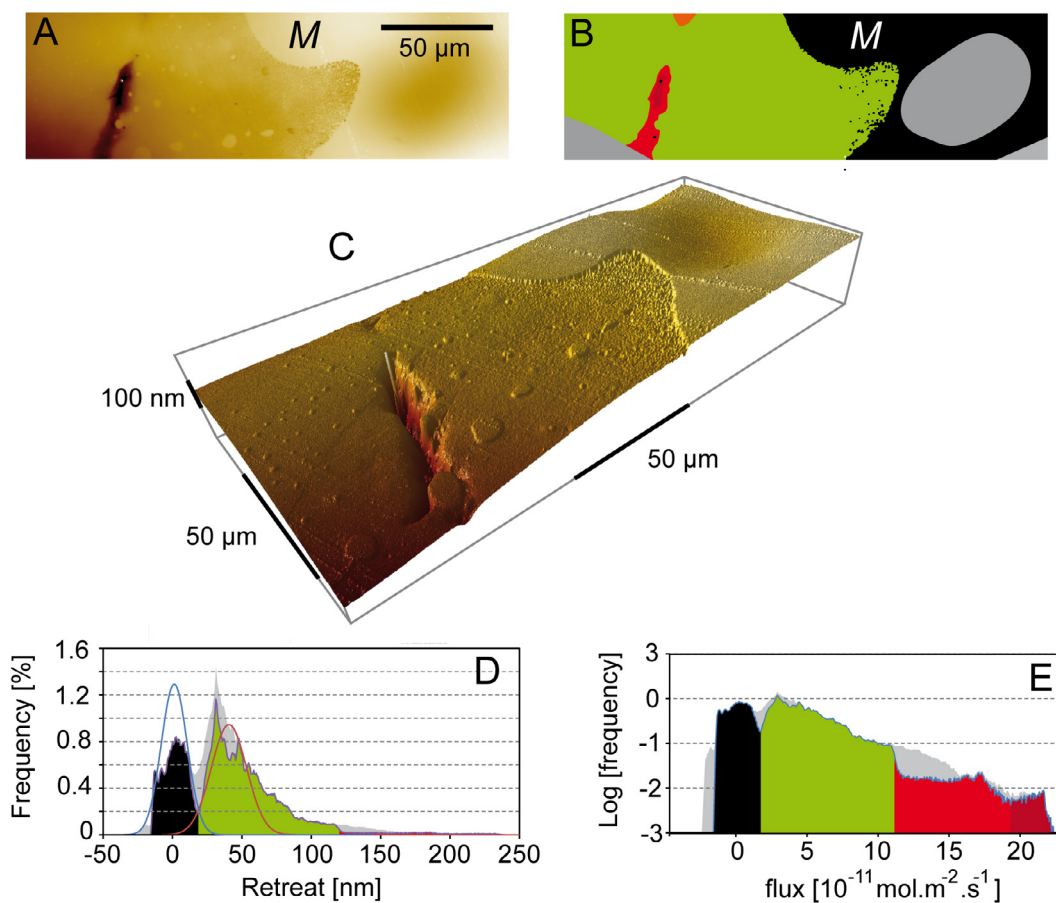


Fig. 6. Surface topography of an olivine reactivity probe after 9 months of incubation in the A horizon of the soil profile of the plot (A, C). Interpretation of surface topography as weathering fluxes (B) estimated from topography and rate spectra (D, E), following the approach developed in (Fischer et al., 2012). Zones impacted by global surface retreat (green) with respect to initial masked surface area (black, M) and local alteration features (red). The contribution of zones related to the initial topography is highlighted in grey. (For interpretation of the references to colour in this figure legend, the reader is referred to the web version of this article.)

communities on mineral weathering and the effect of extrinsic factors on mineralosphere development are specifically addressed for contrasted compartment of the CZ.

#### 4.1. Contribution of intrinsic and extrinsic factors to the field-laboratory discrepancy

Field weathering rates of individual minerals are usually determined with indirect methods. In this study, nanoscale topography variations were used to directly probe mineral dissolution rates in the field (Figs. 5, 6 and 10). A major finding is that up to two orders of magnitude separate field measurements and laboratory-based predictions (see Tables 1 and 2) from WITCH. Our *in-situ* measurements confirmed lower field weathering rates determined using indirect methods, although fresh surfaces (laboratory-type samples) were used here. The contribution of intrinsic and extrinsic factors to this discrepancy are discussed below.

##### 4.1.1. Contribution of intrinsic surface aging

Surface aging refers to any physicochemical modification of the surface of an altered silicate contributing to the decline of its dissolution rate. Surface aging has been

suggested to be an intrinsic factor that contributes to the field-lab discrepancy (Daval et al., 2017, 2018; Fischer et al., 2012; Gruber et al., 2014; Lüttge et al., 2013; Nugent et al., 1998; White and Brantley, 2003). We designed the present study to ensure that surface aging was unlikely to significantly affect dissolution rates of probed minerals.

Indeed, polished mineral surfaces used to probe *in-situ* dissolution rates of fresh silicate surfaces in the field minimized the contribution of intrinsic factors to the field-laboratory discrepancy. Assuming that aging (and the possible formation of passivation layers) requires a minimal portion of mineral surface to be weathered (in agreement with recent studies such as Gin et al. (2015) or Daval et al. (2018)), the reaction progress ( $\xi$ ) after which it becomes significant (i.e., beyond the uncertainties of the measurement), should be specific to the considered mineral at given conditions. Reaction progress ( $\xi$ ) quantifies here the extent of the reaction of dissolution (in  $\text{mol}\cdot\text{m}^{-2}$ ) for either olivine or labradorite. In a recent study, Wild et al. (2016) reported that the decline of labradorite dissolution rate related to surface ageing was observed for  $\xi \geq 2.54 \times 10^{-3} \text{ mol}\cdot\text{m}^{-2}$ . Regarding olivine, mineral age-

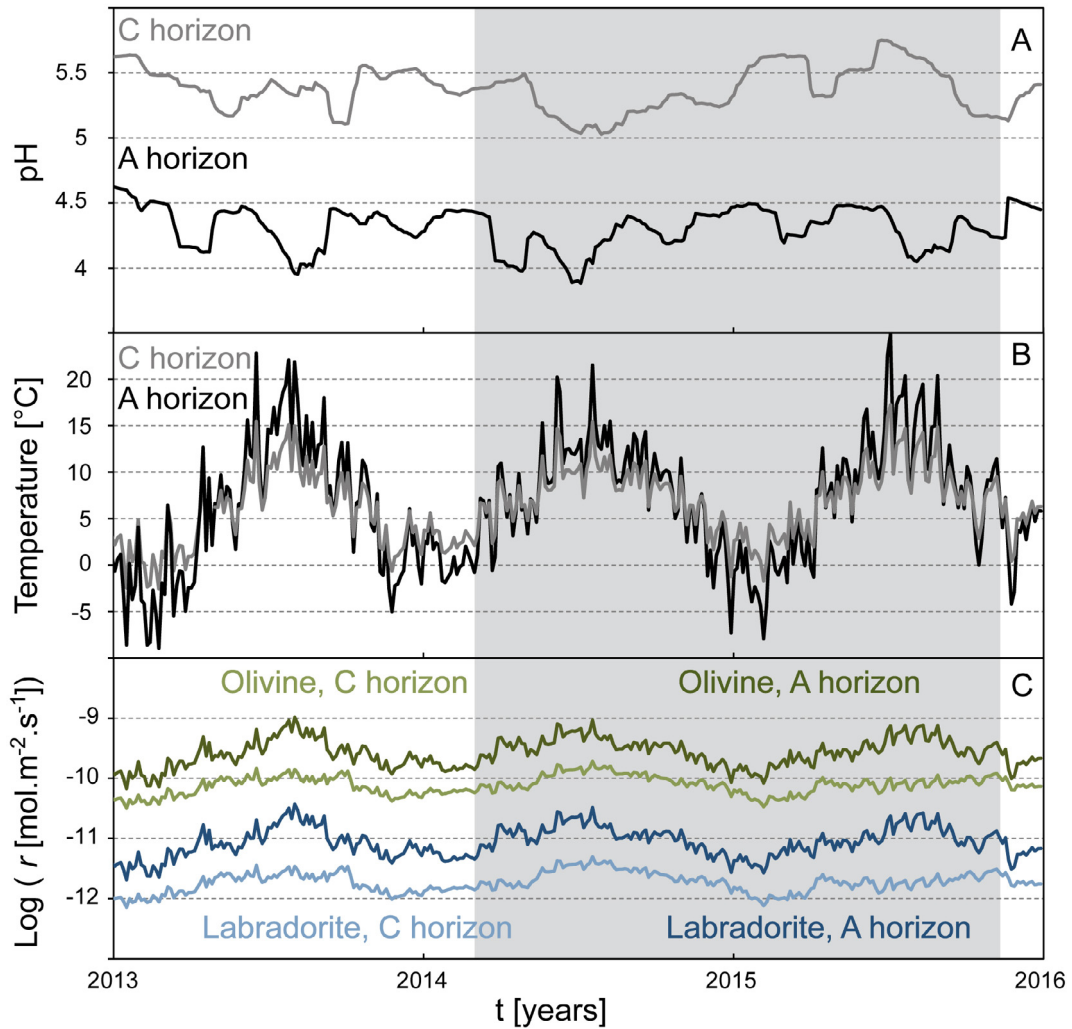


Fig. 7. Temporal variations of pH (A), temperature (B), and dissolution rates (C) of olivine and labradorite modeled by WITCH for two soil horizons at the beech plot of the Strengbach catchment. The greyed areas correspond to the incubation period of the probes.

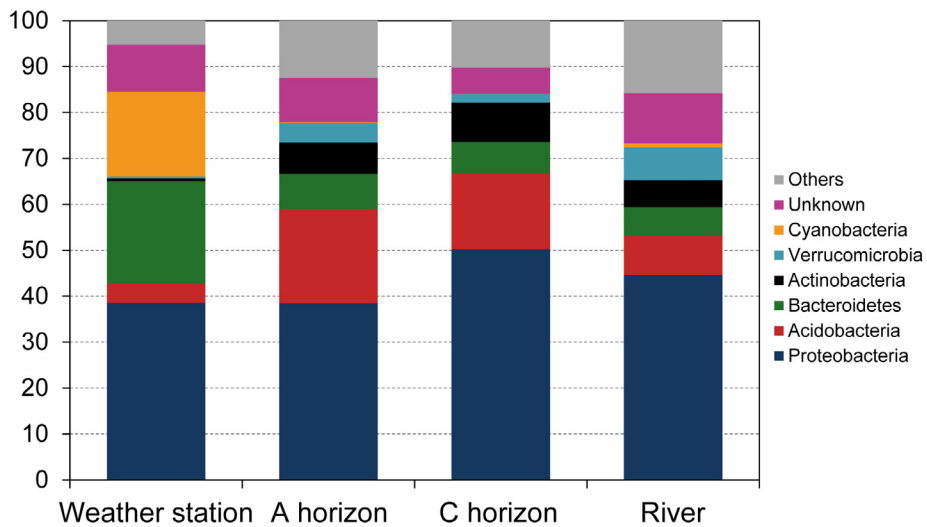


Fig. 8. Relative proportions of bacterial phyla analyzed in the environmental probes incubated in several compartments of the critical zone at the Strengbach catchment. Mean values over all samples incubated at a given location. “Others” category gathers the 20 less represented phyla together with sequences which could not be classified with a sufficient degree of confidence.

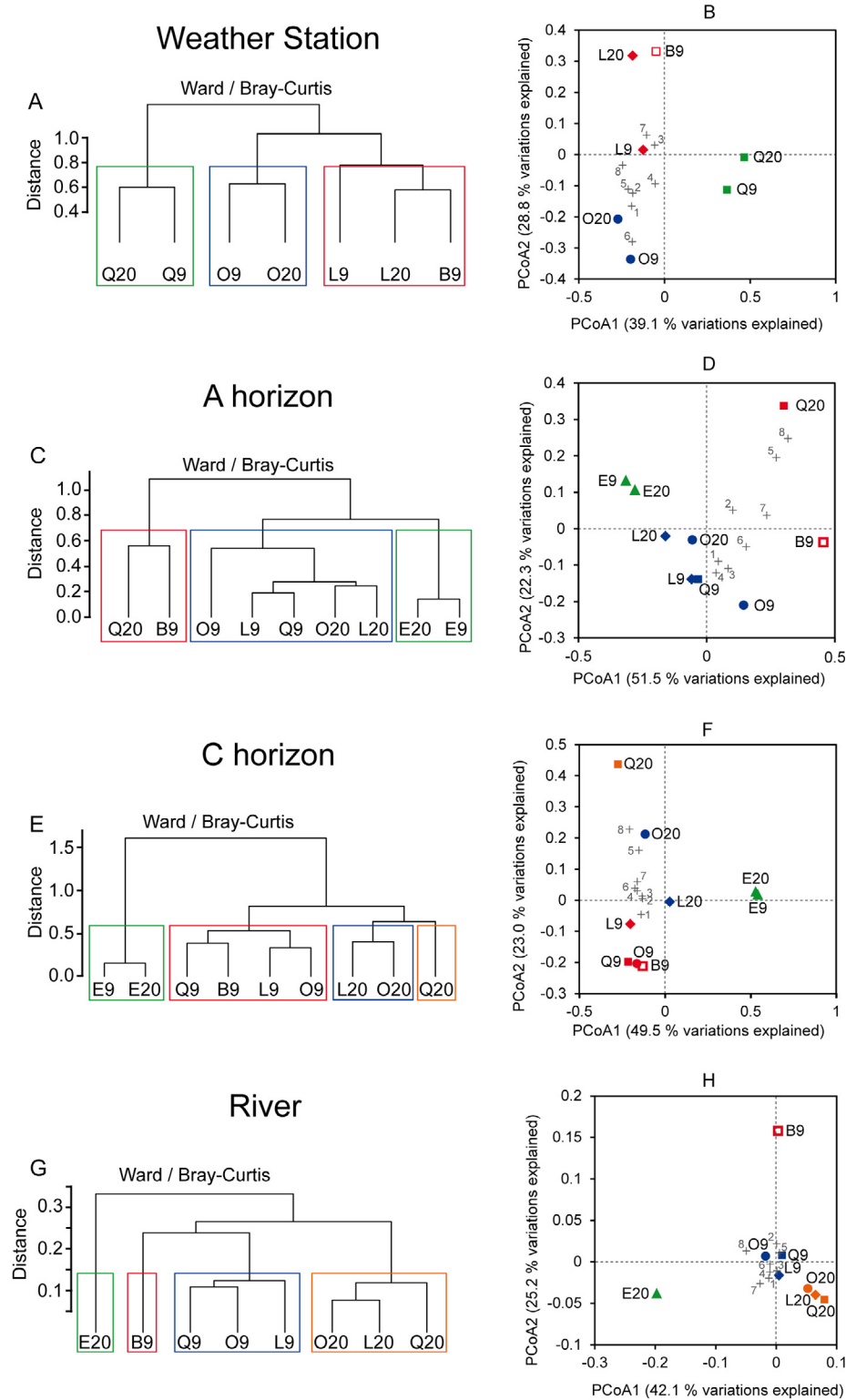


Fig. 9. Statistical analyses of the composition of microbial communities of the environmental probes incubated at the weather station (A,B), in the A horizon (C,D), in the C horizon (E,F), and in the stream (G,H) after 9 and 20 months of incubation. Samples from the mineralosphere of labradorite (L), olivine (O) and quartz (Q), as well as microbial communities from environmental matrices (E, either soil or stream sediments) and empty test bags (B) after 9 and 20 months of incubation. Trees correspond to the aggregation of OTUs at the species level with the Ward method on the basis of Bray-Curtis distances (A, C, E, G). Principal coordinate analyses (PCoA) of the relative abundance of the 16S rRNA genes with colors corresponding to the clusters determined with the Ward method. Crosses match to a *posteriori* projection of OTUs corresponding to *Collimonas* sp. (1), *Burkholderia* sp. (2), *Pseudomonas* sp. (3), *Janthinobacterium* sp. (4), *Leifsonia* sp. (5), *Polaromonas* sp. (6), *Sphingomonas* sp. (7), *Arthrobacter* sp. (8).



ing was evidenced in laboratory conditions for  $\xi \geq 6.92 \cdot 10^{-2} \text{ mol}\cdot\text{m}^{-2}$  (Daval et al., 2011). As reported in Tables 1 and 2, the maximum reaction progress expected for labradorite and olivine, calculated as the product of the dissolution rate times the incubation period, reached  $\xi = 5.68 \cdot 10^{-4} \text{ mol}\cdot\text{m}^{-2}$  (labradorite altered into the A horizon over 20 months) and  $\xi = 1.71 \cdot 10^{-2} \text{ mol}\cdot\text{m}^{-2}$  (olivine altered into the A horizon over 20 months), respectively, which are below the threshold limit reported above. Hence, any difference between the measured and the modeled reaction rates can be attributed to extrinsic factors. In addition, fresh labradorite powders incubated in the A horizon of the exact same plot for durations exceeding four years were still far from being completely covered with passivating surface layers (Daval et al., 2018), thereby further supporting this assertion. *In-situ* measurements could thus be directly compared with WITCH estimates that rely on kinetic rate laws obtained from laboratory experiments.

#### 4.1.2. Extrinsic factors in the laboratory-field discrepancy

Dissolution rates depend on extrinsic parameters, as emphasized in the simplified version of Eq. (5), adapted from (Lasaga, 1998):

$$R_{min} = A \cdot \exp\left(\frac{-E_{a,min}^i}{RT}\right) \cdot a_{H^+}^n \cdot f(\Delta G_{r,sil}) \quad (9)$$

describing mineral weathering rate  $R_{min}$  as a function of temperature  $T$ , the Gibbs free energy with respect to silicate (*sil*) dissolution  $\Delta G_{r,sil}$ , and the pH of the fluid, quantified by the chemical activity of protons ( $a_{H^+}^n$ ). These three parameters are the main extrinsic factors that control the aqueous mineral dissolution rate. Aside from the gas constant  $R$ , the other parameters of this equation, such as the Arrhenius pre-exponential factor  $A$ , the activation energy  $E_{a,min}^i$ , and the reaction order  $n$  are constants derived from laboratory experiments, which are specific to the considered dissolution reaction.

A wide range of values has been reported for each of these three parameters, even for the same mineral (Palandri and Kharaka, 2004). Such disparities in parameter values can lead to significant uncertainties between predicted mineral dissolution rates (Rimstidt et al., 2012). Parameters chosen for the present study were retrieved from Rosso and Rimstidt (2000) data for olivine ( $A = 3.467 \text{ mol}\cdot\text{m}^{-2}\cdot\text{s}^{-1}$ ,  $E_a = 42.6 \text{ kJ}\cdot\text{mol}^{-1}$ , and  $n = 0.50$ ) and Palandri and Kharaka (2004) data for labradorite ( $A = 0.321 \text{ mol}\cdot\text{m}^{-2}\cdot\text{s}^{-1}$ ,  $E_a = 42.1 \text{ kJ}\cdot\text{mol}^{-1}$ , and  $n = 0.63$ ). These two studies provide a meta-analysis of experimental kinetic data and apply statistical methods to infer the rate parameters reported above. We verified that the corresponding rate laws satisfactorily predict dissolution rates of the labradorite and olivine powders reacted in mixed flow set-ups, using the soil solutions collected from lysimetric plates at the Strengbach catchment (see details in Wild et al. (2018)).

As temperature is an input parameter of the numerical simulations, it can be ruled out as a factor explaining the field-laboratory discrepancy. Since simulated pH values were either similar to those measured, or slightly higher,

the contribution of this parameter to the minimal field-lab discrepancy reported in Tables 1 and 2 is negligible. Hence, the observed field-laboratory discrepancy can be ascribed either to the effect of  $\Delta G_{r,sil}$  quantified by the  $f(\Delta G_{r,sil})$  function, or to the fluid-mineral contact time, which is an implicit condition to Eq. (9).

Surface retreats could only be distinguished in areas where fluid circulation occurred on labradorite and olivine samples (see Section 3.2 and Figs. 3 and 4, respectively). This indicates that extent and duration of fluid-mineral contact may partly account for the field-laboratory discrepancy. In terms of spatial extent of the fluid-mineral interface, no compact coating of secondary minerals potentially masking significant portion of mineral surface could be observed on mineral surfaces after incubation. This hypothesis was therefore ruled out.

The extent of fluid-mineral contact time is, on the other hand, indirectly implemented in WITCH with the soil moisture saturation factor (*SMS*) given in Eq. (4). *SMS* estimates the proportion of the bulk soil volume saturated with aqueous solution for a given depth, which corresponds to the proportion of minerals that is susceptible to exchange matter with the fluid. However, the *SMS* does not allow to localize fluid circulation zones at the soil profile scale. The discrepancy between observations and model outputs (Fig. 11) is unlikely to result from the hydrological budget alone since the concentration of conservative tracers, such as sulfate anions, fitted observation for the A-horizon (see Section 2.5 and Table A.5). Surface retreats measured for mineral probes of the stream sets were at best one order of magnitude lower than those estimated with kinetic rate laws derived from laboratory experiments, despite permanent fluid-mineral contact (Tables 1 and 2).

The effect of the Gibbs free energy of reaction on mineral dissolution rate may contribute to explain the field-lab discrepancy. The dependence of mineral dissolution rate on  $\Delta G_{r,sil}$  is implemented in WITCH through the  $(1 - \Omega^S)$  term in Eq. (5), in agreement with the transition state theory (TST), which is equivalent to:

$$f_1(\Delta G_r) = 1 - \left[ \exp\left(\frac{\Delta G_r}{RT}\right) \right]^S \quad (10)$$

in Eq. (9). Even though this relation is widely used in reactive transport codes and sometimes successfully applied to reproduce field observations (Godd eris and Donnadi eu, 2009; Godderis et al., 2006; Violette et al., 2010), it may not be appropriate to describe complex reaction pathways (Gin et al., 2008). For instance, the sum of two parallel reactions, with a transition from far-to-equilibrium to close-to-equilibrium dissolution regime occurring at  $\Delta G_r = -7.5 \text{ kcal}\cdot\text{mol}^{-1}$ , better described the dissolution kinetics of labradorite (Taylor et al., 2000). To test the effect of the selection of the  $f(\Delta G_{r,sil})$  function, the empirical relation of Taylor et al. (2000) was implemented in WITCH:

$$f_2(\Delta G_r) = \left\{ \begin{array}{l} 0.76 * \left[ 1 - \exp\left(-1.3 * 10^{-17} * \left(\frac{|\Delta G_r|}{RT}\right)^{14}\right) \right] \\ + 0.24 * \left[ 1 - \exp\left(-0.35 * \frac{|\Delta G_r|}{RT}\right) \right] \end{array} \right\} \quad (11)$$

with the exception of a minor sign correction (the original paper indicates  $-0.24$  instead of  $+0.24$  for Eq. (11)). Temporal variations of the  $f_1$  and  $f_2$  functions for the A and C horizons are shown in Fig. 11 A.  $\Delta G_{r,sil}$  did not affect labradorite dissolution rate in the soil profile if one considers the  $f_1$  function. In contrast, a significant decrease of the apparent dissolution rate of labradorite in the C horizon occurred using the  $f_2$  function. Regarding the C horizon, changing the  $f(\Delta G_{r,sil})$  function for the  $f_2$  function resolved the field-laboratory discrepancy for labradorite, as shown by values of  $\Delta_{L/F} < 1$  (parenthesis, Table 1) and in agreement with Gruber et al. (2014). For the A-horizon, however, the field-laboratory discrepancy could not be totally explained by the equilibrium term since the discrepancy persisted ( $\Delta_{L/F} > 1$ ). Regarding olivine, in the absence of an alternative function describing the  $R_{min} - \Delta G_{r,sil}$  dependence of its dissolution kinetics, the TST-based law was used by default, although it may not be fully relevant.

Overall, this shows that current models may partly fail to capture the effects of both heterogeneity of fluid circulations and local physicochemical conditions on mineral dissolution rates in soils of the CZ. The presence of microorganisms associated to minerals may be one of the factors influencing both fluid circulation and local physicochemical conditions. The relationship between bacterial communities and minerals in various compartments of the CZ is discussed below.

#### 4.2. The effect of microorganisms on mineral weathering in the CZ

Amongst other extrinsic parameters, biota has been shown to affect mineral weathering (Ahmed and Holmstrom, 2015; Bonneville et al., 2009; Courty et al., 2010; Li et al., 2016; Uroz et al., 2009). Most strikingly, the weathering rate for the olivine surface incubated for 9 months at the weather station was low, corresponding to a retreat  $< 1$  nm (Table 2), whereas the surface incubated for 20 months exhibited an exceptional retreat of up to

172 nm (Fig. 10), corresponding to a field-laboratory discrepancy value of  $\Delta_{L/F} = 1$  (no discrepancy, see Table 2). Rainwater cannot be considered as the unique weathering agent for olivine because open-air incubation conditions offer rather homogeneous input weathering conditions. Variations of reaction rates are at odds with the exposure of olivine surface to homogeneous reactive fluids at the weather station. In addition, the mineral surface retreat measured after 20 months would virtually correspond to a permanent interaction of the mineral with a fluid of average composition of the rainwater. This condition is unlikely as the samples incubated at the weather stations were prone to drying-wetting cycles. In addition, permanent fluid interaction is inconsistent with the retreat observed after 9 months of incubation in the same conditions (sample MO9, Table 2). The occurrence of several microorganisms on the meteoric probes supports the hypothesis that organisms contributed to mineral weathering.

Microorganisms can also affect locally fluid circulation in soil (Or et al., 2007), which can impact mineral weathering by regulating fluid-mineral contact. More specifically, biofilms can disrupt interactions between mineral surface and bulk fluid and stabilize locally zones of preferential fluid circulation. Here, samples from the A-horizon show that the flow path of the solution can be precisely constrained around the fluid boundary ( $\pm 10$   $\mu\text{m}$ , approximate width of the transition zone indicated by dashed lines in Fig. 4G) (Fig. 4D–F). Biofilms may thus subtly control fluid flow and act similarly to the RTV glue used to estimate global surface retreat (dark grey area, Fig. 4C and striped area, Fig. 4D–F and H).

While biofilm may have increased the dissolution rate of olivine exposed to meteoric fluid or indirectly contributed to the field-lab discrepancy by affecting fluid-mineral contact, direct observation of mineral-microorganism contact is missing to support such hypothesis.

Concerning soil compartments, no clear direct evidence of bacterial weathering could be observed despite biological weathering could have been favored by K, Ca and Mg

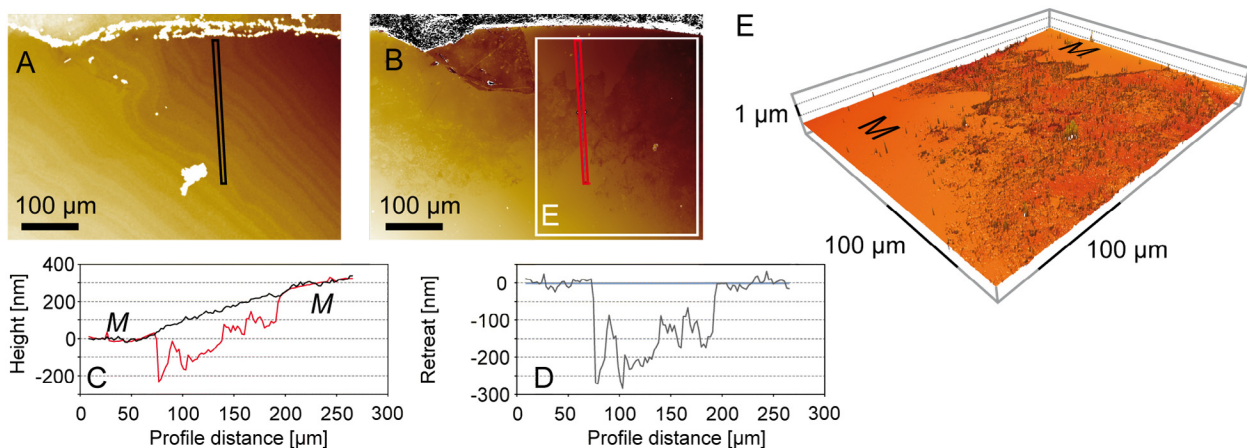


Fig. 10. Detail of the surface topography of an olivine reactivity probe before (A) and after (B) 20 months of incubation at the weather station. Superposition of profiles before (black) and after (red) incubation (C) and corresponding surface retreat (D). 3D plot of the surface after incubation (B) with masked (M) zones (E).

concentrations typical for nutrient-poor pedological systems (van der Heijden et al., 2013). Mg concentrations in the soil profile (Fig. 2) were similar to those observed in a reference forest plot located in the Morvan Mountains (Burgundy, France), which exhibited Mg-deficiency thirty years after clear-cutting native forest (van der Heijden et al., 2013). Moreover, symptoms of forest decline, and Mg and Ca nutritional deficits in trees were already described at the Strengbach catchment (Dambrine et al., 1992). We thus tried to indirectly probe clues possible mineral-bacteria interactions by tracking the development of mineral-specific bacterial communities, and how their composition varied according to the mineral substrates (Jones and Bennett, 2014) or their dissolution rates (Uroz et al., 2012). The influence of minerals on bacterial communities in their direct vicinity and the potential for mineral weathering of bacterial phylotypes found in the environmental probe are discussed below. However, one has to keep in mind that only about 6% of the bacterial phyla are identified by usual taxonomic databases (Solden et al., 2016; Yarza et al., 2014). Therefore, relating weathering fluxes to specific bioweathering bacteria in the field solely based on their phylogenetic affiliation remains an elusive goal. In this exploratory study, the relevance of bacterial diversity as a potential indicator of the mineral-bacteria interactions was evaluated.

#### 4.2.1. Establishment of mineral-specific bacterial communities

Our results are consistent with the hypothesis that incubated minerals host specific mineralosphere bacterial communities. Indeed, mineralosphere bacterial communities from the soil profile or the Strengbach stream differed from those of the corresponding bulk soil or stream sediment samples respectively. Similarly, mineral-specific communities from the meteoric sets established according to the mineral type. This is in agreement with previous results obtained with a similar approach using *in-situ* incubation of fresh minerals (Mitchell et al., 2013; Uroz et al., 2012), field samples (Gleeson et al., 2006), or microcosms inoculated with microbial consortia from a forest soil (Heckman et al., 2013). This point is highlighted here since the development of mineral-specific bacterial communities may reflect the development of phylotypes adapted to mineral weathering, along with the development of bioweathering processes adapted to the mineral substrate.

Interestingly, our results also show that mineralosphere communities changed over time. While previous studies provided “snapshots” of mineralosphere bacterial communities (Mitchell et al., 2013; Uroz et al., 2012), two incubation times were considered in the present approach (9 and 20 months), which constitutes an attempt to address temporal changes of bacterial communities. In the C soil horizon and stream sets of probes, time rather than intrinsic mineral weatherability seemed to constitute a primary factor driving community composition (Fig. 9E). In probes from the C horizon, bacterial communities associated with olivine and labradorite differed more from those associated with non-reactive samples (quartz) after 20 months of incubation than in the initial stages of the mineralosphere forma-

tion (i.e., after 9 months). This supports the idea that the mineralosphere develops according to mineral reactivity under field conditions, even though more probes and replicates in each CZ compartments are necessary to confirm this trend.

#### 4.2.2. Influence of extrinsic factors on mineralosphere development

Comparison of environmental probes incubated in the atmospheric, soil and stream compartments of the CZ revealed the effect of extrinsic factors (i.e., not related to the mineral) on mineralosphere bacterial communities. Altogether, the results suggest that the relative contribution of extrinsic *versus* intrinsic factors on the differentiation of bacterial communities increases across CZ compartments, following a meteoric < C-horizon < A-horizon < stream pattern.

The meteoric sets of probes were exclusively exposed to atmospheric inputs, which are intermittent and nutrient-poor compared to those recorded in the soil or in the stream. In soils, the hygrometry and cationic inputs may be buffered by secondary mineral phases. By contrast, the composition of the fluid in direct contact with mineral probes in the stream was rapidly controlled by the stream hydrochemistry. In the case of the meteoric sets of probes, the mineral type was expected to largely control the surface environment, and thus the response of bacterial communities. Indeed, the mineral represented the main source of inorganic nutrients and/or toxic elements, such as Al (Jones and Bennett, 2014; Singh et al., 2005). Lower overall bacterial diversity for the meteoric sets of probes compared to other sets, and distinct bacterial communities (Fig. 9A) and diversity (Fig. A.3) according to the mineral substrate, support this hypothesis. The lower impact of external inputs in the case of meteoric probes may also explain the rapid differentiation of bacterial communities according to the mineral type, regardless of the incubation time.

Contrasting with observations from the C horizon and meteoric sets of probes, bacterial communities from the A horizon did not cluster according to mineral type. This may reflect more dynamic conditions in the A horizon with respect to both physicochemical conditions and microbial diversity. This is suggested by heterogeneous flows on the probe surface (Figs. 3 and 4). On the short term, organic matter cycling and bioturbation (Gutiérrez and Jones, 2006) may particularly affect microorganisms of the A horizon by altering nutrient inputs or physicochemical parameters. This may tremendously confound and delay the response of microbial communities to mineral reactivity.

The effect of extrinsic factors was apparently even stronger in the case of the stream probes because fluid circulation directly and continuously impacted the physicochemical characteristics of the incubation environment (T, pH, etc.). This is emphasized by similar composition of bacterial communities in the stream set of probes (Fig. 9H) and higher bacterial diversity observed on these samples compared to other compartments (Fig. A.3). In this case, continuous inputs of dissolved nutrients and particle-associated biomass (Fig. 1J) may interfere with the mineralosphere development. This may in turn challenge and

delay the detection of a mineralosphere effect (i.e., specific bacterial communities associated to specific minerals). Analogous effects were observed in an oceanic context, where minerals incubated close to hydrothermal discharge (providing a continuous input of nutrient from fluids) only served as a solid support on which bacteria could attach, whereas similar minerals located far from these fluids inputs served as Fe source for microorganisms (Henri et al., 2016). As a result, the effect of extrinsic factors on the differentiation of mineralosphere bacterial communities may largely differ among CZ compartments for similar incubation times.

#### 4.2.3. Occurrence of potential mineral-weathering bacteria

Potential mineral-weathering bacterial taxa found in the environmental probes included *Pseudomonas* sp., *Collimonas* sp., *Burkholderia* sp., *Janthinobacterium* sp., *Leifsonia* sp., and *Arthrobacter* sp. The occurrence of these taxa underscores the potential for biotic alteration in the mineralospheres of the investigated soils. These taxa were found in higher abundance not only in the sets of probes incubated in the soil profile compared to other compartments (2.1% vs. 0.1% on average, Fig. 12), but also in the mineralosphere compared to the corresponding bulk soil horizons (2.6% vs. 0.2% on average, Fig. 12).

*Pseudomonas* sp. dominated the studied mineralospheres, with an average proportion of 2.5% for the whole dataset and of 4.5% in the soil samples (<0.1% for the other compartments of the critical zone). Phylotypes belonging to the *Pseudomonas* genus have been described in the literature for their ability to dissolve biotite (Uroz et al., 2009). For both the A and C horizons of the soil profile, *Pseudomonas* sp. was more abundant on labradorite and olivine samples. The proportion of *Pseudomonas* sp. remained constant over time in samples from the C horizon, whereas it decreased in the A horizon between 9 and 20 months of incubation (Fig. 12). This suggests that *Pseudomonas* sp. pioneered the colonization of the mineral probes of the soil sets, and mainly occurred in relation to saprolitic alteration. This may be due to the significance of rock weathering in the C horizon relative to other processes that may affect microbial assemblages in the A horizon (e.g. bioturbation, degradation of organic matter or nutrient cycling).

*Collimonas* sp. was also particularly abundant in the soil mineral probes (1.9%) compared to other compartments (<0.1%). It has long been thought that bacteria belonging to the *Collimonas* genus live at the expense of organic exudates produced by fungi of the mycorrhizosphere (de Boer et al., 2004). However, *Collimonas* sp. are also capable of extracting elements, such as iron from biotite (Calvaruso et al., 2007; Uroz et al., 2007), or from granite powders (Lapanje et al., 2012) by producing siderophores and supplying their fungal hosts with inorganic nutrients. In our samples, *Collimonas* sp. was found in a larger proportion in the C horizon (i.e., in contact with the saprolite) than in the organic-rich A horizon.

The projection of *Collimonas* sp. found for each of the corresponding PCoA analyses (Fig. 9) revealed similar trends for samples from the two soil horizons. *Collimonas* sp. prevailed on quartz and labradorite after 9 months of

incubation, whereas it decreases in all samples between 9 and 20 months, except for olivine, where it increases over the same period. The decline of *Collimonas* sp. was associated to increasing bacterial diversity in all sets of probes incubated in the soil, except for quartz in the A horizon (Fig. A.3). This suggests that *Collimonas* sp. may first establish at the fungus-rock interface, before specializing in iron extraction through the production of siderophores.

On average, *Burkholderia* sp. accounted for 1.0% of the total genera recovered from the probes. *Burkholderia* sp. have been reported to enhance the dissolution of biotite, like some members of the genus *Collimonas* (Calvaruso et al., 2007; Uroz et al., 2007), but also apatite (Lepleux et al., 2012; Mailloux et al., 2009), phosphate minerals (Kim et al., 2005; Vassilev et al., 2006), quartz (Ullman et al., 1996), bytownite (Barker et al., 1998; Welch et al., 1999) and other feldspars (Ullman et al., 1996), and more generally granite (Wu et al., 2008) or basalt (Wu et al., 2007). Similarly to *Collimonas* sp., *Burkholderia* sp. was mainly found in soil compartments, especially in the A horizon, in particular associated to the quartz sample incubated for 20 months. The latter sample also exhibits a notably low bacterial diversity ( $H' < 5$  and  $I < 50$ , Fig. A.3). *Burkholderia* sp. therefore seems to correspond to “lithophilic” bacteria particularly adapted to the context of the A horizon.

*Janthinobacterium* sp., *Leifsonia* sp. and *Arthrobacter* sp., which have been described for their ability to dissolve granite through the production of oxalic acid and hydrogen cyanide (Frey et al., 2010), also belonged to the first decile of most abundant bacterial genera. Biotite dissolution was enhanced by species of the genus *Janthinobacterium* (Uroz et al., 2009). Species belonging to the genus *Arthrobacter* may promote the dissolution of hornblende (Kalinowski et al., 2000), quartz and feldspars (Ullman et al., 1996), including bytownite (Barker et al., 1998; Welch et al., 1999). The proportions of *Leifsonia* sp. and *Arthrobacter* sp. after 9 months was higher in the C horizon compared to the A horizon, whereas the proportions were larger in quartz samples after 20 months in both soil horizons (Fig. 12). *Leifsonia* sp., or *Arthrobacter* sp. may preferentially adapt to environments with a lower influence of extrinsic factors, like in the C horizon compared to the A horizon (see Section 4.2.2 and Fig. 12), or to the quartz surface, not releasing any toxic or valuable elements. This results in high apparent proportion for samples associated to low diversity, such as the quartz samples. *Janthinobacterium* sp. occurred in a larger proportion in probes from the C horizon, in particular on olivine and labradorite probes that bear elements of interest such as Mg, Fe or Ca (Fig. 12). The population decrease between 9 and 20 months of incubation suggests that *Janthinobacterium* sp. may be “lithophilic” and compete with other bacterial processes, as described above.

Finally, *Polaromonas* sp., which was previously reported in the context of granite weathering (Frey et al., 2010), was present in high proportions in all sets of probes of the C horizon.

Overall, bacterial communities of mineralosphere of the soil profile feature several populations that may be involved

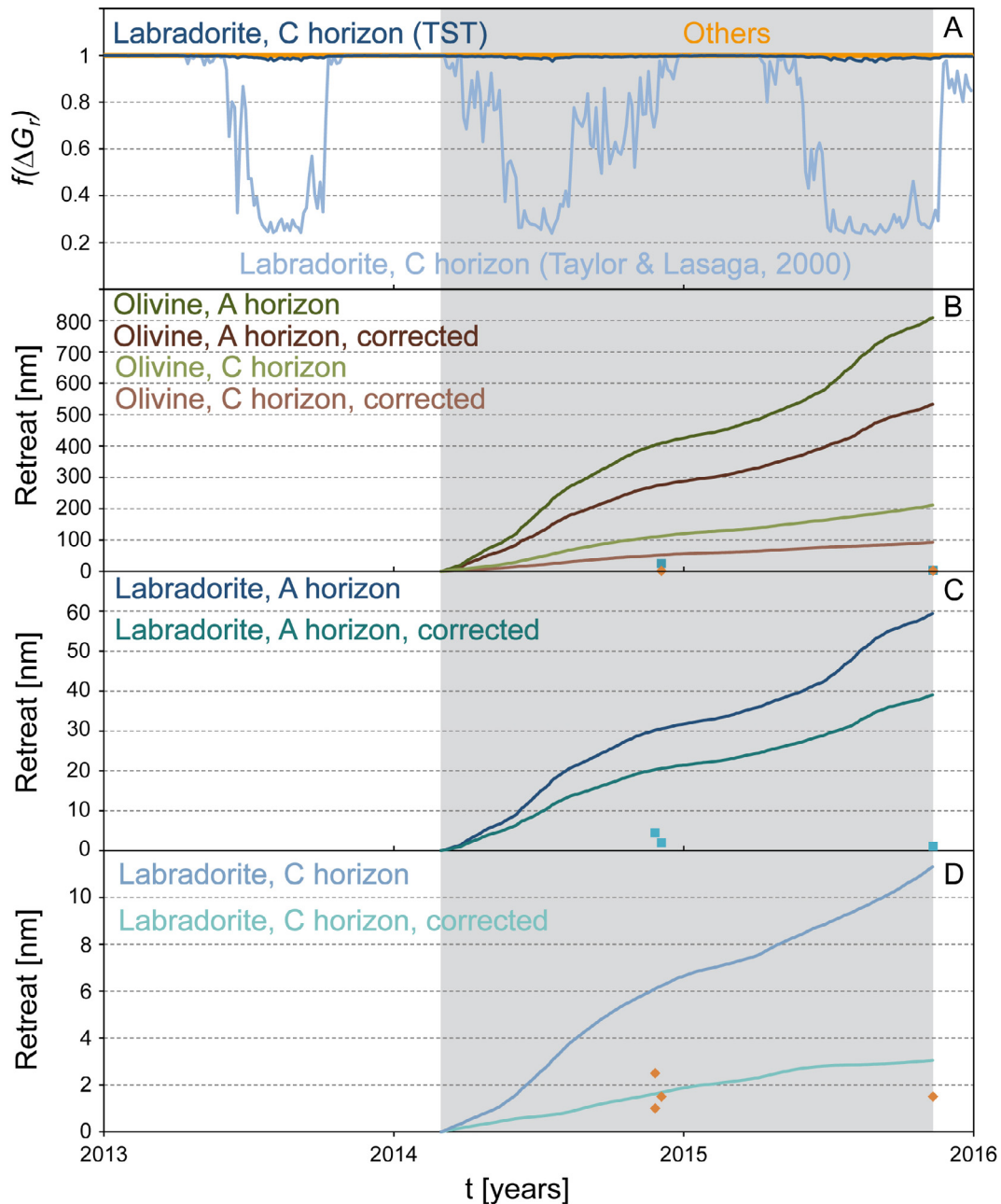


Fig. 11. Temporal change of the  $f(\Delta G_r)$  term describing the effect of the distance from equilibrium of the solution on mineral dissolution rate (A), and of the surface retreats for olivine and labradorite predicted by the WITCH model for the A and C horizons of the soil profile (B–D). The period highlighted in grey corresponds to the incubation of the samples. The  $f(\Delta G_r)$  function is equal to  $\sim 1$  for all conditions except for labradorite in the C horizon when the  $rate - \Delta G_r$  relation is described by the model of Taylor et al. (2000). Squares and diamonds in panels (B)–(D) represent *measured* surface retreats for samples incubated in the A and C horizons, respectively. Continuous curves represent *predicted* surface retreats based on outputs from the WITCH model. Corrected curves take into account fluid-mineral contact time and are based on  $f_2(\Delta G_r)$  function (see text). This figure stresses the amplitude of the field-laboratory discrepancy. The error bars are smaller than the size of symbols.

in mineral weathering. The distribution of bacterial taxa putatively associated with mineral weathering coincided with the disturbed bacterial pattern of the A horizon. Indeed, extrinsic factors (i.e. factors influencing the bacterial community that are not related to the mineral sub-

strate) may considerably affect the distribution of the taxa potential associated with mineral weathering, such as *Pseudomonas* sp., *Janthinobacterium* sp., *Leifsonia* sp., or *Arthrobacter* sp. Such disturbances may delay the development of a mineralosphere specific to the mineral type.

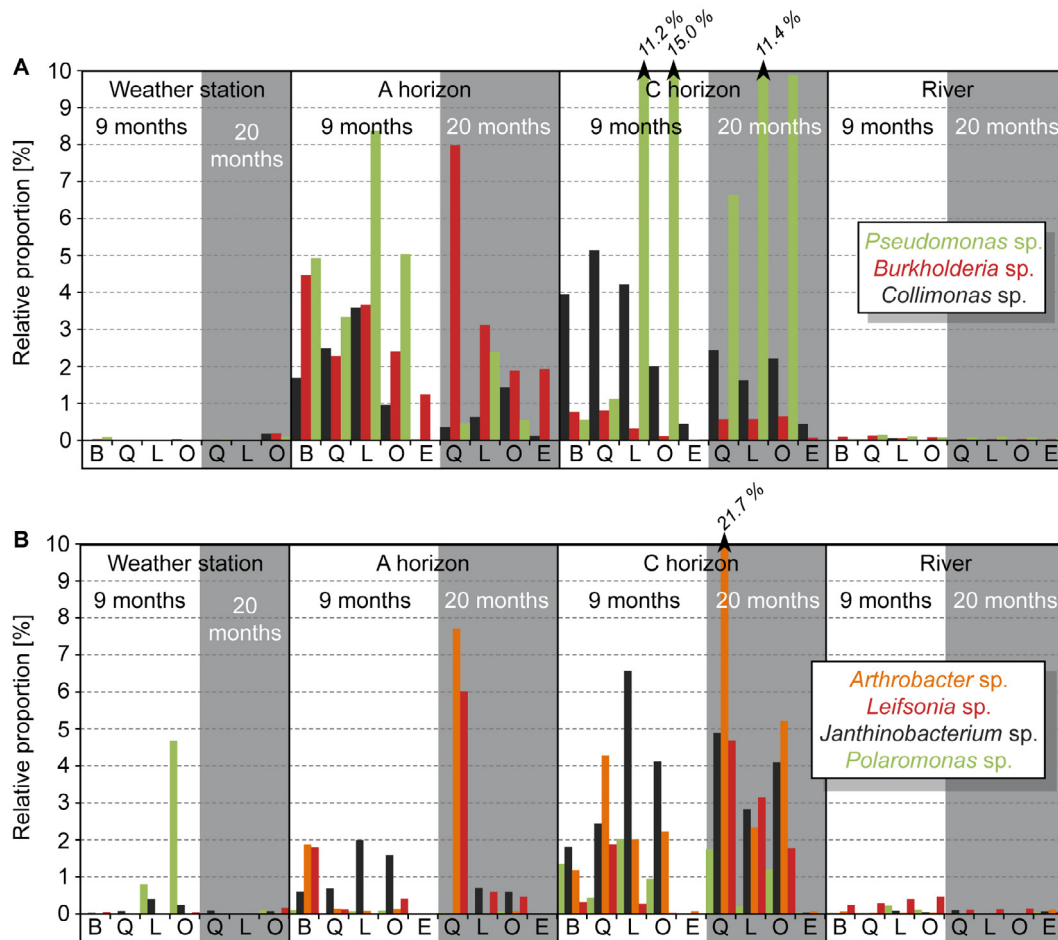


Fig. 12. Relative proportions of *Pseudomonas* sp., *Burkholderia* sp., *Collimonas* sp. (A), and *Arthrobacter* sp., *Leifsonia* sp., *Janthinobacterium* sp., et *Polaromonas* sp. (B), in the mineralospheres of quartz (Q), labradorite (L) and olivine (O), as well as in environmental samples (E) or empty bags (B). This figure illustrates that the proportion of genera known for their mineral weathering ability in pedological context is increased in the microbial communities of the environmental probes compared to those recovered from their respective surrounding environmental matrix.

#### 4.2.4. Do bacteria with weathering abilities actively dissolve minerals?

Determining whether microorganisms with known weathering activity and present at the surface of minerals actively contribute to mineral dissolution remains challenging. While to date most of the evidences of bacterial mineral dissolution have been based on microscopic observations (Bennett et al., 2001; Jongmans et al., 1997), this approach is still controversial (Benzerara et al., 2007). Another methodology has been suggested, which considers a linear relationship between *in-situ* weathering rates and bacterial diversity (Uroz et al., 2012). In our case, however, no clear correlation could be established between the extent of mineral weathering and bacterial diversity or enrichment of specific taxa (i.e., *Collimonas* sp., *Burkholderia* sp., *Pseudomonas* sp., *Janthinobacterium* sp., *Leifsonia* sp., or *Arthrobacter* sp.). These specific taxa, which may be functionally related to mineral weathering, do not necessarily express this function, and their occurrence may not necessarily reflect a selective pressure for their bioweathering ability.

Nevertheless, regarding samples exposed to open-air weathering at the weather station, bacterial diversity globally increases with increasing mineral weatherability (quartz < labradorite < olivine), irrespective of the mineral incubation time. This supports the clustering of bacterial communities according to the mineral substrate shown in Fig. 9A. In the A-horizon, the Shannon and inverse Simpson diversity indices are higher for olivine (the most weatherable mineral) incubated 20 months in the A horizon than for all the other mineral samples of this compartment (Fig. A.3). The potential for nutrient mobilization of a given mineral may thus stimulate competition between bioweathering agents and support diverse bacterial communities.

Regarding the C horizon, variation in the diversity indices echoes the cluster analysis (Fig. 9E). This stresses the first-order importance of time on the composition of bacterial communities. Indeed, time prevailed over the type of the mineral in the C horizon. Globally, diversity increased for all three minerals as a function of time. On the other hand, diversity was significantly higher for

“reactive” minerals after 20 months of incubation and reached that of the corresponding soil samples (Fig. A.3A, B). Bacterial richness (Chao 1 index) was only significantly higher for labradorite after 20 months, which reflected the diversification of bacterial communities in the C horizon for minerals. The low differences of bacterial diversity between mineral samples immersed in the Strengbach stream confirms the second-order role played by mineral substrates for this compartment.

To conclude, diversity analysis of bacterial communities for samples incubated in the A and C horizons of the soil profile and at the weather station suggests a relationship between microbial community diversity and mineral reactivity. Our results support the hypothesis that mineral substrates, depending on their incubation context, may affect microbial communities in their mineralospheres. Diversity analysis of bacterial communities suggests that potential bioweathering bacteria of the A horizon are preferentially associated to (Mg, Fe)-bearing phases, such as olivine, whereas those of the C horizon are rather associated to feldspars minerals, such as labradorite. However, this study is not fully conclusive as to whether the potential of bacterial weathering is actually expressed. This would require strengthening the statistical significance of the results by increasing the number of probes and replicates on the one hand, and to statistically relate dissolution features to bioweathering processes on the other. To address this issue, future studies may consider imaging spatial distribution of microorganisms on mineral samples, especially by assessing their distance from the surface or from dissolution “hot spots” with confocal laser scanning microscopy. Once microorganisms are located on the mineral surface, possible associated dissolution features of biotic origin may be used to quantify associated “biotic rates” by rate spectra analysis (Fischer et al., 2012), as presented on Fig. 6.

## 5. SUMMARY AND CONCLUSIONS

The present study shows that *in-situ* mineral dissolution rates and bioweathering environments of minerals can be directly probed *in-situ* in contrasted compartments of the CZ. This approach is complementary to those already used to estimate mineral weathering rates in the field, as it allows for the estimation of mineral weathering rates over short timescales (from months to years).

In spite of the limited number of samples that could be incubated, fundamental parameters to understand mineral dissolution in the CZ were identified. In particular, extrinsic factors may partly explain the gap existing between estimates of silicate dissolution rates obtained in the laboratory and in the field, while potential bioweathering bacteria were found in all CZ compartments. Salient results of the present study can be summarized as follows:

- 1) In A and C soil horizons, simulated dissolution rates converted into global surface retreats were greater by a factor of 1 to 270 for olivine, and of 2 to 54 for labradorite than those measured *in-situ*.

- 2) The heterogeneity of fluid circulation in soil profiles should be accounted for in chemical weathering models as it can significantly affect *in-situ* mineral weathering rates.
- 3) The effect of the Gibbs free energy of reaction on labradorite dissolution rates partly explains the discrepancy between laboratory estimates and field measurements for the A and C soil horizons.
- 4) The nature of the mineral substrate affects bacterial communities of the mineralosphere. This process can however be affected or delayed by extrinsic factors, such as nutrient or biomass inputs mediated by fluid circulation.

In parallel, our study also raised some issues that need to be explored in the future. Potential bioweathering bacterial phylotypes were detected on environmental probes incubated in A and C horizons. However, bioweathering activities could not be proved, and the contribution of bacterial activities to the total weathering flux could not be quantified. The approach proposed in this study may however be generalized to evaluate *in-situ* expression of microbial bioweathering functions (i) to quantify the effect of microbial communities on mineral dissolution rate, and (ii) to gradually include bacteria/mineral interactions in next-generation chemical weathering models.

Finally, incubation of a greater number of integrative reactivity probes of various mineral types may help in the future to unravel effective local reaction conditions controlling *in-situ* mineral reactivity in CZ compartments.

## ACKNOWLEDGEMENT

The fabrication of probes and of the experimental setup benefited from the technical support of Lisa Wild and René Wild who are warmly acknowledged. The follow up of the experiment would not have been possible without the help of the OHGE team, and particularly Solenn Cotel and Sylvain Benarioumlil. Authors also wish to thank Michael Heap, Heline Maison and Gilles Morvan for technical assistance and François Guyot for numerous and fruitful discussions that contributed to this manuscript. This work was funded through a grant to Gwenaél Imfeld for the project MicXtreme under the framework of the LabEx G-EAU-THERMIE PROFONDE project ANR-11-LABX-0050, and through a grant to Damien Daval under the framework of the VALVE project (EC2CO-BIOHEFFECT program coordinated by the CNRS-Institut National des Sciences de l'Univers).

## APPENDIX A. SUPPLEMENTARY MATERIAL

Supplementary data to this article can be found online at <https://doi.org/10.1016/j.gca.2019.01.003>.

## REFERENCES

- Ackerer J., Chabaux F., Van der Woerd J., Viville D., Pelt E., Kali E., Lerouge C., Ackerer P., Roupert R. D. and Negrel P. (2016) Regolith evolution on the millennial timescale from combined

- U-Th-Ra isotopes and in situ cosmogenic Be-10 analysis in a weathering profile (Strengbach catchment, France). *Earth Planet. Sci. Lett.* **453**, 33–43.
- Ahmed E. and Holmstrom S. J. M. (2015) Microbe-mineral interactions: The impact of surface attachment on mineral weathering and element selectivity by microorganisms. *Chem. Geol.* **403**, 13–23.
- Alisa Mast M. and Drever J. I. (1987) The effect of oxalate on the dissolution rates of oligoclase and tremolite. *Geochim. Cosmochim. Acta* **51**, 2559–2568.
- Altschul S. F., Gish W., Miller W., Myers E. W. and Lipman D. J. (1990) Basic local alignment search tool. *J. Mol. Biol.* **215**, 403–410.
- Alveteg M. (1998). Dynamics of forest soil chemistry. Ph.D, Lund University.
- Arvidson R. S., Ertan I. E., Amonette J. E. and Lutge A. (2003) Variation in calcite dissolution rates: A fundamental problem? *Geochim. Cosmochim. Acta* **67**, 1623–1634.
- Arvidson R. S. and Lutge A. (2010) Mineral dissolution kinetics as a function of distance from equilibrium - New experimental results. *Chem. Geol.* **269**, 79–88.
- Augusto L., Turpault M. P. and Ranger J. (2000) Impact of forest tree species on feldspar weathering rates. *Geoderma* **96**, 215–237.
- Babcsanyi I., Meite F. and Imfeld G. (2017) Biogeochemical gradients and microbial communities in Winogradsky columns established with polluted wetland sediments. *FEMS Microbiol. Ecol.*, 93.
- Barker W. W. and Banfield J. F. (1996) Biologically versus inorganically mediated weathering reactions: Relationships between minerals and extracellular microbial polymers in lithobiontic communities. *Chem. Geol.* **132**, 55–69.
- Barker W. W., Welch S. A., Chu S. and Banfield J. F. (1998) Experimental observations of the effects of bacteria on aluminosilicate weathering. *Am. Miner.* **83**, 1551–1563.
- Beaulieu E., Godderis Y., Donnadiu Y., Labat D. and Roelandt C. (2012) High sensitivity of the continental-weathering carbon dioxide sink to future climate change. *Nat. Clim. Change*, **2**, 346–349.
- Beaulieu E., Godderis Y., Labat D., Roelandt C., Oliva P. and Guerrero B. (2010) Impact of atmospheric CO<sub>2</sub> levels on continental silicate weathering. *Geochim. Cosmochim. Acta* **74**, A65–A65.
- Beig M. S. and Lutge A. (2006) Albite dissolution kinetics as a function of distance from equilibrium: Implications for natural feldspar weathering. *Geochim. Cosmochim. Acta* **70**, 1402–1420.
- Bennett P. C., Hiebert F. K. and Choi W. J. (1996) Microbial colonization and weathering of silicates in a petroleum-contaminated groundwater. *Chem. Geol.* **132**, 45–53.
- Bennett P. C., Rogers J. R. and Choi W. J. (2001) Silicates, silicate weathering, and microbial ecology. *Geomicrobiol. J.* **18**, 3–19.
- Benzerara K., Menguy N., Banerjee N. R., Tyliczszak T., Brown G. E. and Guyot F. (2007) Alteration of submarine basaltic glass from the Ontong Java Plateau: A STXM and TEM study. *Earth Planet. Sci. Lett.* **260**, 187–200.
- Bonneau M., Dambrine E., Nys C. and Range r. J. (1991) Apports acides et cycles des cations et de l'azote : quelques reflexions à partir des dispositifs de Monthermé (Ardennes) et d'Aubure (Vosges). *Sci. du Sol* **29**, 125–145.
- Bonneville S., Bray A. W. and Benning L. G. (2016) Structural Fe (II) oxidation in biotite by an ectomycorrhizal fungi drives mechanical forcing. *Environ. Sci. Technol.* **50**, 5589–5596.
- Bonneville S., Smits M. M., Brown A., Harrington J., Leake J. R., Brydson R. and Benning L. G. (2009) Plant-driven fungal weathering: Early stages of mineral alteration at the nanometer scale. *Geology* **37**, 615–618.
- Brantley S. L., Liermann L., Bau M. and Wu S. (2001) Uptake of trace metals and rare earth elements from hornblende by a soil bacterium. *Geomicrobiol. J.* **18**, 37–61.
- Bray R. J. and Curtis J. T. (1957) An ordination of the upland forest communities in southern Wisconsin. *Ecol. Monogr.* **27**, 325–349.
- Brunauer S., Emmet P. H. and Teller E. (1938) Adsorption of gases in multimolecular layers. *Journal of the American Chemical Society* **60**, 309–319.
- Calvaruso C., Turpault M.-P., Leclerc E. and Frey-Klett P. (2007) Impact of ectomycorrhizosphere on the functional diversity of soil bacterial and fungal communities from a forest stand in relation to nutrient mobilization processes. *Microb. Ecol.* **54**, 567–577.
- Carroll S. A. and Knauss K. G. (2005) Dependence of labradorite dissolution kinetics on CO<sub>2</sub>(aq), Al(aq), and temperature. *Chem. Geol.* **217**, 213–225.
- Certini G., Campbell C. D. and Edwards A. C. (2004) Rock fragments in soil support a different microbial community from the fine earth. *Soil Biology & Biochemistry* **36**, 1119–1128.
- Courty P. E., Buee M., Diedhiou A. G., Frey-Klett P., Le Tacon F., Rineau F., Turpault M. P., Uroz S. and Garbaye J. (2010) The role of ectomycorrhizal communities in forest ecosystem processes: New perspectives and emerging concepts. *Soil Biol. Biochem.* **42**, 679–698.
- Collignon C., Uroz S., Turpault M. P. and Frey-Klett P. (2011) Seasons differently impact the structure of mineral weathering bacterial communities in beech and spruce stands. *Soil Biology and Biochemistry* **43**, 2012–2022.
- Dambrine E., Carisey N., Pollier B. and Granier A. (1992) Effects of drought on the yellowing status and the dynamic of mineral elements in the xylem sap of a declining spruce stand (*Picea abies* Karst.). *Plant Soil* **150**, 303–306.
- Daval D., Bernard S., Rémusat L., Wild B., Guyot F., Micha J. S., Rieutord F., Magnin V. and Fernandez-Martinez A. (2017) Dynamics of altered surface layer formation on dissolving silicates. *Geochim. Cosmochim. Acta* **209**, 51–69.
- Daval D., Calvaruso C., Guyot F. and Turpault M.-P. (2018) Time-dependent feldspar dissolution rates resulting from surface passivation: Experimental evidence and geochemical implications. *Earth Planet. Sci. Lett.* **498**, 226–236.
- Daval D., Hellmann R., Saldi G. D., Wirth R. and Knauss K. G. (2013) Linking nm-scale measurements of the anisotropy of silicate surface reactivity to macroscopic dissolution rate laws: New insights based on diopside. *Geochim. Cosmochim. Acta* **107**, 121–134.
- Daval D., Sissmann O., Menguy N., Saldi G. D., Guyot F., Martinez I., Corvisier J., Garcia B., Machouk I., Knauss K. G. and Hellmann R. (2011) Influence of amorphous silica layer formation on the dissolution rate of olivine at 90°C and elevated pCO<sub>2</sub>. *Chem. Geol.* **284**, 193–209.
- Davison W. and Seed G. (1983) The kinetics of the oxidation of ferrous iron in synthetic and natural-waters. *Geochim. Cosmochim. Acta* **47**, 67–79.
- de Boer W., Leveau J. H. J., Kowalchuk G. A., Gunnewiek P., Abeln E. C. A., Figge M. J., Sjollem K., Janse J. D. and van Veen J. A. (2004) *Collimonas fungivorans* gen. nov., sp nov., a chitinolytic soil bacterium with the ability to grow on living fungal hyphae. *Int. J. Syst. Evol. Microbiol.* **54**, 857–864.
- Drever J. I. and Stillings L. L. (1997) The role of organic acids in mineral weathering. *Colloids. Surf. A Physicochem. Eng. Asp.* **120**, 167–181.
- Duplay J., Semhi K., Errais E., Imfeld G., Babcsanyi I. and Perrone T. (2014) Copper, zinc, lead and cadmium bioavailability and retention in vineyard soils (Rouffach, France): The impact of cultural practices. *Geoderma* **230**, 318–328.



- El Gh'Mari A. (1995) *Etude minéralogique, pétrophysique et géochimique de la dynamique d'altération d'un granite soumis au dépôts atmosphériques acides (Bassin Versant du Strengbach, Vosges, France)*, PhD. Université Louis Pasteur.
- Esther J., Sukla L. B., Pradhan N. and Panda S. (2015) Fe (III) reduction strategies of dissimilatory iron reducing bacteria. *Korean J. Chem. Eng.* **32**, 1–14.
- Feger K.-H., Brahmner G. and Zöttl H. W. (1990) An integrated watershed/plot-scale study of element cycling in spruce ecosystems of the black forest. *Water, Air, Soil Pollut.* **54**, 545–560.
- Ferrier K. L., Kirchner J. W., Riebe C. S. and Finkel R. C. (2010) Mineral-specific chemical weathering rates over millennial timescales: Measurements at Rio Icacos, Puerto Rico. *Chem. Geol.* **277**, 101–114.
- Fischer C., Arvidson R. S. and Lüttge A. (2012) How predictable are dissolution rates of crystalline material? *Geochim. Cosmochim. Acta* **98**, 177–185.
- Frey B., Rieder S. R., Brunner I., Ploetze M., Koetzsch S., Lapanje A., Brandl H. and Furrer G. (2010) Weathering-associated bacteria from the Damma glacier forefield: physiological capabilities and impact on granite dissolution. *Appl. Environ. Microbiol.* **76**, 4788–4796.
- Gaillardet J., Dupre B. and Allegre C. J. (1995) A global mass budget applied to the Congo basin rivers - Erosion rates and continental crust composition. *Geochim. Cosmochim. Acta* **59**, 3469–3485.
- Gaillardet J., Dupré B., Louvat P. and Allègre C. J. (1999) Global silicate weathering and CO<sub>2</sub> consumption rates deduced from the chemistry of large rivers. *Chem. Geol.* **159**, 3–30.
- Ganor J., Renznik I. J. and Rosenberg Y. O. (2009) Organics in water-rock interactions, Thermodynamics and kinetics of water-rock interaction. *Mineral. Soc. America*, 259–369.
- Gerard F., Clement A., Fritz B. and Crovisier J. L. (1996) Introduction of transport phenomena into the thermo-kinetic code KINDIS: The code KIRMAT. *C. R. Acad. Sci., Serie II. Sciences de la Terre et des Planetes* **322**, 377–384.
- Gin S., Jegou C., Frugier P. and Minet Y. (2008) Theoretical consideration on the application of the Aagaard-Helgeson rate law to the dissolution of silicate minerals and glasses. *Chem. Geol.* **255**, 14–24.
- Gin S., Jollivet P., Fournier M., Angeli F., Frugier P. and Charpentier T. (2015) Origin and consequences of silicate glass passivation by surface layers. *Nat. Commun.* **6**, 6360.
- Gleeson D. B., Kennedy N. M., Clipson N., Melville K., Gadd G. M. and McDermott F. P. (2006) Characterization of bacterial community structure on a weathered pegmatitic granite. *Microb. Ecol.* **51**, 526–534.
- Goddéris Y. and Donnadieu Y. (2009) Climatic plant power. *Nature* **460**, 40.
- Goddéris Y., Francois L. M., Probst A., Schott J., Moncoulon D., Labat D. and Viville D. (2006) Modelling weathering processes at the catchment scale: The WITCH numerical model. *Geochim. Cosmochim. Acta* **70**, 1128–1147.
- Granier A., Breda N., Biron P. and Villette S. (1999) A lumped water balance model to evaluate duration and intensity of drought constraints in forest stands. *Ecol. Model.* **116**, 269–283.
- Gruber C., Zhu C., Georg R. B., Zakon Y. and Ganor J. (2014) Resolving the gap between laboratory and field rates of feldspar weathering. *Geochim. Cosmochim. Acta* **147**, 90–106.
- Gutiérrez J. L. and Jones C. G. (2006) Physical ecosystem engineers as agents of biogeochemical heterogeneity. *BioScience* **56**, 227–236.
- Gleeson D. B., Clipson N., Melville K., Gadd G. M. and McDermott F. P. (2005) Characterization of fungal community structure on a weathered pegmatitic granite. *Microbial Ecology* **50**, 360–368.
- Harris I., Jones P. D., Osborn T. J. and Lister D. H. (2014) Updated high-resolution grids of monthly climatic observations - the CRU TS3.10 dataset. *Int. J. Climatol.* **34**, 623–642.
- Heckman K., Welty-Bernard A., Vazquez-Ortega A., Schwartz E., Chorover J. and Rasmussen C. (2013) The influence of goethite and gibbsite on soluble nutrient dynamics and microbial community composition. *Biogeochemistry* **112**, 179–195.
- Hedrich S., Schlomann M. and Johnson D. B. (2011) The iron-oxidizing proteobacteria. *Microbiol.-Sgm* **157**, 1551–1564.
- Hellmann R. and Tisserand D. (2006) Dissolution kinetics as a function of the Gibbs free energy of reaction: An experimental study based on albite feldspar. *Geochim. Cosmochim. Acta* **70**, 364–383.
- Henri P. A., Rommevaux-Jestin C., Lesongeur F., Mumford A., Emerson D., Godfroy A. and Ménez B. (2016) Structural iron (II) of basaltic glass as an energy source for zetaproteobacteria in an abyssal plain environment, off the mid Atlantic ridge. *Front Microbiol.*, 6.
- Johnson J., Aherne J. and Cummins T. (2015) Base cation budgets under residue removal in temperate maritime plantation forests. *For. Ecol. Manage.* **343**, 144–156.
- Johnstone T. C. and Nolan E. M. (2015) Beyond iron: non-classical biological functions of bacterial siderophores. *Dalton Trans.* **44**, 6320–6339.
- Jones A. A. and Bennett P. C. (2014) Mineral microniches control the diversity of subsurface microbial populations. *Geomicrobiol. J.* **31**, 246–261.
- Jongmans A. G., vanBremen N., Lundstrom U., vanHees P. A. W., Finlay R. D., Srinivasan M., Unestam T., Giesler R., Melkerud P. A. and Olsson M. (1997) Rock-eating fungi. *Nature* **389**, 682–683.
- Kalinowski B. E., Liermann L. J., Brantley S. L., Barnes A. and Pantano C. G. (2000) X-ray photoelectron evidence for bacteria-enhanced dissolution of hornblende. *Geochim. Cosmochim. Acta* **64**, 1331–1343.
- Kim Y. H., Bae B. and Choung Y. K. (2005) Optimization of biological phosphorus removal from contaminated sediments with phosphate-solubilizing microorganisms. *J. Biosci. Bioeng.* **99**, 23–29.
- Klaminder J., Lucas R. W., Futter M. N., Bishop K. H., Kohler S. J., Egnell G. and Laudon H. (2011) Silicate mineral weathering rate estimates: Are they precise enough to be useful when predicting the recovery of nutrient pools after harvesting? *For. Ecol. Manage.* **261**, 1–9.
- Knauss K. G. and Wolery T. J. (1988) The dissolution kinetics of quartz as a function of pH and time at 70°C. *Geochim. Cosmochim. Acta* **52**, 43–53.
- Lapanje A., Wimmersberger C., Furrer G., Brunner I. and Frey B. (2012) Pattern of elemental release during the granite dissolution can be changed by aerobic heterotrophic bacterial strains isolated from Damma glacier (central Alps) deglaciated granite sand. *Microb. Ecol.* **63**, 865–882.
- Lasaga A. C. (1998) *Kinetic Theory in the Earth Sciences*. Princeton University Press, New York.
- Lefèvre Y. (1988) Les sols du bassin versant d'Aubure : caractérisation et facteurs de répartition. *Ann. Sci. For.* **45**, 417–422.
- Lepleux C., Turpault M. P., Oger P., Frey-Klett P. and Uroz S. (2012) Correlation of the abundance of betaproteobacteria on mineral surfaces with mineral weathering in forest soils. *Appl. Environ. Microbiol.* **78**, 7114–7119.
- Li Z. B., Liu L. W., Chen J. and Teng H. H. (2016) Cellular dissolution at hypha- and spore-mineral interfaces revealing unrecognized mechanisms and scales of fungal weathering. *Geology* **44**, 319–322.

- Lower S. K., Hochella M. F. and Beveridge T. J. (2001) Bacterial recognition of mineral surfaces: nanoscale interactions between *Shewanella* and  $\alpha$ -FeOOH. *Science* **292**, 1360–1363.
- Lucas R. W., Klaminder J., Futter M. N., Bishop K. H., Egnell G., Laudon H. and Hogberg P. (2011) A meta-analysis of the effects of nitrogen additions on base cations: Implications for plants, soils, and streams. *For. Ecol. Manage.* **262**, 95–104.
- Lüttge A., Arvidson R. S. and Fischer C. (2013) A stochastic treatment of crystal dissolution kinetics. *Elements* **9**, 183–188.
- Maher K., DePaolo D. J. and Lin J. C.-F. (2004) Rates of silicate dissolution in deep-sea sediment: In situ measurement using  $^{234}\text{U}/^{238}\text{U}$  of pore fluids. *Geochim. Cosmochim. Acta* **68**, 4629–4648.
- Maher K., Steefel C. I., White A. F. and Stonestrom D. A. (2009) The role of reaction affinity and secondary minerals in regulating chemical weathering rates at the Santa Cruz Soil Chronosequence, California. *Geochim. Cosmochim. Acta* **73**, 2804–2831.
- Mailloux B. J., Alexandrova E., Keimowitz A. R., Wovkulich K., Freyer G. A., Herron M., Stolz J. F., Kenna T. C., Pichler T., Polizzotto M. L., Dong H., Bishop M. and Knappett P. S. K. (2009) Microbial mineral weathering for nutrient acquisition releases arsenic. *Appl. Environ. Microbiol.* **75**, 2558–2565.
- Mitchell A. C., Lafreniere M. J., Skidmore M. L. and Boyd E. S. (2013) Influence of bedrock mineral composition on microbial diversity in a subglacial environment. *Geology* **41**, 855–858.
- Negrel P., Allegre C. J., Dupre B. and Lewin E. (1993) Erosion sources determined by inversion of major and trace element ratios and strontium isotopic ratios in river water - The congo basin case. *Earth Planet. Sci. Lett.* **120**, 59–76.
- Newman D. K. and Kolter R. (2000) A role for excreted quinones in extracellular electron transfer. *Nature* **405**, 94–97.
- Nugent M. A., Brantley S. L., Pantano C. G. and Maurice P. A. (1998) The influence of natural mineral coatings on feldspar weathering. *Nature* **395**, 588–591.
- Odum E. P. (1950) Bird populations of the Highlands (North Carolina) plateau in relation to plant succession and avian invasion. *Ecology* **31**, 587–605.
- Oksanen J., F. Blanchet G., Kindt R., Legendre P., Minchin P. R., O'Hara R. B., Simpson G. L., Solymos P., Stevens M. H. H. and Wagner H. (2013) Vegan: Community Ecology Package. R package version 2.0-8, <http://CRAN.R-project.org/package=vegan>.
- Or D., Phutane S. and Dechesne A. (2007) Extracellular polymeric substances affecting pore-scale hydrologic conditions for bacterial activity in unsaturated soils. *Vadose Zone J.* **6**, 298–305.
- Paces T. (1983) Rate constants of dissolution derived from the measurements of mass balance in hydrological catchments. *Geochim. Cosmochim. Acta* **47**, 1855–1863.
- Palandri J. L., Kharaka Y. K. (2004). A compilation of rate parameters of water-mineral interaction kinetics for application to geochemical modeling, in: Survey, U.S.G. (Ed.), U.S. Geological Survey, Open File Report. U.S. Geological Survey, Open File Report, p. 70.
- Pierret M. C., Stille P., Prunier J., Viville D. and Chabaux F. (2014) Chemical and U-Sr isotopic variations in stream and source waters of the Strengbach watershed (Vosges mountains, France). *Hydrol. Earth Syst. Sci.* **18**, 3969–3985.
- Prunier J., Chabaux F., Stille P., Gangloff S., Pierret M. C., Viville D. and Aubert A. (2015) Geochemical and isotopic (Sr, U) monitoring of soil solutions from the Strengbach catchment (Vosges mountains, France): Evidence for recent weathering evolution. *Chem. Geol.* **417**, 289–305.
- Reguera G., McCarthy K. D., Mehta T., Nicoll J. S., Tuominen M. T. and Lovley D. R. (2005) Extracellular electron transfer via microbial nanowires. *Nature* **435**, 1098–1101.
- Rimstidt J. D., Brantley S. L. and Olsen A. A. (2012) Systematic review of forsterite dissolution rate data. *Geochim. Cosmochim. Acta* **99**, 159–178.
- Roden E. E., Kappler A., Bauer I., Jiang J., Paul A., Stoesser R., Konishi H. and Xu H. F. (2010) Extracellular electron transfer through microbial reduction of solid-phase humic substances. *Nat. Geosci.* **3**, 417–421.
- Roelandt C., Godderis Y., Bonnet M. P. and Sondag F. (2010) Coupled modeling of biospheric and chemical weathering processes at the continental scale. *Global Biogeochem. Cycles* **24**.
- Rogers J. R. and Bennett P. C. (2004) Mineral stimulation of subsurface microorganisms: release of limiting nutrients from silicates. *Chem. Geol.* **203**, 91–108.
- Rosso J. J. and Rimstidt D. J. (2000) A high resolution study of forsterite dissolution rates. *Geochim. Cosmochim. Acta* **64**, 797–811.
- Saha R., Saha N., Donofrio R. S. and Bestervelt L. L. (2013) Microbial siderophores: a mini review. *J. Basic Microbiol.* **53**, 303–317.
- Singh R., Beriault R., Middaugh J., Hamel R., Chenier D., Appanna V. D. and Kalyuzhnyi S. (2005) Aluminum-tolerant *Pseudomonas fluorescens*: ROS toxicity and enhanced NADPH production. *Extremophiles* **9**, 367–373.
- Sitch S., Smith B., Prentice I. C., Arneeth A., Bondeau A., Cramer W., Kaplan J. O., Levis S., Lucht W., Sykes M. T., Thonicke K. and Venevsky S. (2003) Evaluation of ecosystem dynamics, plant geography and terrestrial carbon cycling in the LPJ dynamic global vegetation model. *Glob. Chang. Biol.* **9**, 161–185.
- Solden L., Lloyd K. and Wrighton K. (2016) The bright side of microbial dark matter: lessons learned from the uncultivated majority. *Curr. Opin. Microbiol.* **31**, 217–226.
- Steefel C. and Lasaga A. C. (1994) A coupled model for transport of multiple chemical species and kinetic precipitation/dissolution reactions with application to reactive flow in single phase hydrothermal systems. *Am J. Sci.* **294**, 529–592.
- Sverdrup H. (1990) *The kinetics of Chemical Weathering*. Lund University Press, Lund, Sweden.
- Sverdrup H. and Warfvinge P. (1993) Calculating field weathering rates using a mechanistic geochemical model PROFILE. *Appl. Geochem.* **8**, 273–283.
- Sverdrup H. and Warfvinge P. (1995) Estimating field weathering rates using laboratory kinetics. *Chem. Weathering Rates Silicate Miner.*, 485–541.
- Schloss P. D., Westcott S. L., Ryabin T., Hall J. R., Hartmann M., Hollister E. B., Lesniewski R. A., Oakley B. B., Parks D. H., Robinson C. J., Sahl J. W., Stres B., Thallinger G. G., Van Horn D. J. and Weber C. F. (2009) Introducing mothur: Open-Source, Platform-Independent, Community-Supported Software for Describing and Comparing Microbial Communities. *Appl. Environ. Microbiol.* **75**, 7537–7541.
- Taylor A. S., Blum J. D. and Lasaga A. C. (2000) The dependence of labradorite dissolution and Sr isotope release rates on solution saturation state. *Geochim. Cosmochim. Acta* **64**, 2389–2400.
- Tester J. W., Worley W. G., Robinson B. A., Grigsby C. O. and Feerer J. L. (1994) Correlating quartz dissolution kinetics in pure water from 25 to 625°C. *Geochim. Cosmochim. Acta* **58**, 2407–2420.
- Ullman W. J., Kirchman D. L., Welch S. A. and Vandevivere P. (1996) Laboratory evidence for microbially mediated silicate mineral dissolution in nature. *Chem. Geol.* **132**, 11–17.
- Uroz S., Calvaruso C., Turpault M.-P. and Frey-Klett P. (2009) Mineral weathering by bacteria: ecology, actors and mechanisms. *Trends Microbiol.* **17**, 378–387.

- Uroz S., Calvaruso C., Turpault M. P., Pierrat J. C., Mustin C. and Frey-Klett P. (2007) Effect of the mycorrhizosphere on the genotypic and metabolic diversity of the bacterial communities involved in mineral weathering in a forest soil. *Appl. Environ. Microbiol.* **73**, 3019–3027.
- Uroz S., Kelly L. C., Turpault M. P., Lepleux C. and Frey-Klett P. (2015) The Mineralosphere concept: mineralogical control of the distribution and function of mineral-associated bacterial communities. *Trends Microbiol.* **23**, 751–762.
- Uroz S., Turpault M. P., Delaruelle C., Mareschal L., Pierrat J. C. and Frey-Klett P. (2012) Minerals affect the specific diversity of forest soil bacterial communities. *Geomicrobiol.* **J.29**, 88–98.
- van der Heijden G., Legout A., Pollier B., Mareschal L., Turpault M. P., Ranger J. and Dambrine E. (2013) Assessing Mg and Ca depletion from broadleaf forest soils and potential causes - A case study in the Morvan Mountains. *For. Ecol. Manage.* **293**, 65–78.
- van Scholl L., Kuyper T. W., Smits M. M., Landeweert R., Hoffland E. and van Breemen N. (2008) Rock-eating mycorrhizas: their role in plant nutrition and biogeochemical cycles. *Plant Soil* **303**, 35–47.
- Vassilev N., Vassileva M. and Nikolaeva I. (2006) Simultaneous P-solubilizing and biocontrol activity of microorganisms: potentials and future trends. *Appl. Microbiol. Biotechnol.* **71**, 137–144.
- Violette A., Godd ris Y., Mar chal J.-C., Riotte J., Oliva P., Kumar M. S. M., Sekhar M. and Braun J.-J. (2010) Modelling the chemical weathering fluxes at the watershed scale in the Tropics (Mule Hole, South India): Relative contribution of the smectite/kaolinite assemblage versus primary minerals. *Chem. Geol.* **277**, 42–60.
- Viville D., Chabaux F., Stille P., Pierret M. C. and Gangloff S. (2012) Erosion and weathering fluxes in granitic basins: The example of the Strengbach catchment (Vosges massif, eastern France). *Catena* **92**, 122–129.
- Velbel M. A. (1993) Formation of protective surface layers during silicate-mineral weathering under well-leached, oxidizing conditions. *Am. Miner.* **78**, 405–414.
- Walters W. A., Caporaso J. G., Lauber C. L., Berg-Lyons D., Fierer N. and Knight R. (2011) PrimerProspector: de novo design and taxonomic analysis of barcoded polymerase chain reaction primers. *Bioinformatics* **27**, 1159–1161.
- Ward J. H. (1963) Hierarchical grouping to optimize an objective function. *J. Am. Stat. Assoc.* **58**, 236–244.
- Warfvinge P. and Sverdrup H. (1988) Soil liming as a measure to mitigate acid runoff. *Water Resour. Res.* **24**, 701–712.
- Warfvinge P. and Sverdrup H. (1992) Calculating critical loads of acid deposition with PROFILE - a steady-state soil chemistry model. *Water, Air, Soil Pollut.* **63**, 119–143.
- Weber K. A., Achenbach L. A. and Coates J. D. (2006) Microorganisms pumping iron: anaerobic microbial iron oxidation and reduction. *Nat. Rev. Microbiol.* **4**, 752–764.
- Welch S. A., Barker W. W. and Banfield J. F. (1999) Microbial extracellular polysaccharides and plagioclase dissolution. *Geochim. Cosmochim. Acta* **63**, 1405–1419.
- Welch S. A. and Ullman W. J. (1993) The effect of organic acids on plagioclase dissolution rates and stoichiometry. *Geochim. Cosmochim. Acta* **57**, 2725–2736.
- White A. F. and Brantley S. L. (2003) The effect of time on the weathering of silicate minerals: why do weathering rates differ in the laboratory and field? *Chem. Geol.* **202**, 479–506.
- Wild B., Daval D., Guyot F., Knauss K. G., Pollet-Villard M. and Imfeld G. (2016) pH-dependent control of feldspar dissolution rate by altered surface layers. *Chem. Geol.* **442**, 148–159.
- Wild B., Imfeld G., Guyot F. and Daval D. (2018) Early stages of bacterial community adaptation to silicate aging. *Geology* **46**, 555–558.
- Wu L., Jacobson A. D., Chen H.-C. and Hausner M. (2007) Characterization of elemental release during microbe-basalt interactions at T=28 degrees C. *Geochim. Cosmochim. Acta* **71**, 2224–2239.
- Wu L., Jacobson A. D. and Hausner M. (2008) Characterization of elemental release during microbe-granite interactions at T=28 °C. *Geochim. Cosmochim. Acta* **72**, 1076–1095.
- White A. F., Blum A. E., Schulz M. S., Bullen T. D., Harden J. W. and Peterson M. L. (1996) Chemical weathering rates of a soil chronosequence on granitic alluvium. I. Quantification of mineralogical and surface area changes and calculation of primary silicate reaction rates. *Geochim. Cosmochim. Acta* **60**, 2533–2550.
- Yarza P., Yilmaz P., Pruesse E., Glockner F. O., Ludwig W., Schleifer K.-H., Whitman W. B., Euz by J., Amann R. and Rossello-Mora R. (2014) Uniting the classification of cultured and uncultured bacteria and archaea using 16S rRNA gene sequences. *Nat. Rev. Microbiol.* **12**, 635–645.
- Yeh G. T. and Tripathi V. S. (1991) A model for simulating transport of reactive multispecies components: model development and demonstration. *Water Resour. Res.* **27**, 3075–3094.
- Yu C., Lavergren U., Peltola P., Drake H., Bergb ck B. and  str m M. E. (2014) Retention and transport of arsenic, uranium and nickel in a black shale setting revealed by a long-term humidity cell test and sequential chemical extractions. *Chem. Geol.* **363**, 134–144.
- Zhu C., Liu Z., Schaefer A., Wang C., Zhang G., Gruber C., Ganor J. and Georg R. B. (2014) Silicon isotopes as a new method of measuring silicate mineral reaction rates at ambient temperature. *Procedia Earth Planet. Sci.* **10**, 189–193.

Associate editor: Carl Steefel